

# Persistent Scatterer Interferometry analysis of ground deformation in the Po Plain (Piacenza-Reggio Emilia sector, Northern Italy): seismo-tectonic implications

Benedetta Antonielli,<sup>1,2</sup> Oriol Monserrat,<sup>3</sup> Marco Bonini,<sup>4</sup> Nicola Cenni,<sup>5</sup>  
Núria Devanthery,<sup>3</sup> Gaia Righini<sup>6</sup> and Federico Sani<sup>1</sup>

<sup>1</sup>Department of Earth Sciences, University of Florence, via G. La Pira 4, I-50121 Florence, Italy. E-mail: [bene.antonielli@gmail.com](mailto:bene.antonielli@gmail.com)

<sup>2</sup>Tuscan Earth Science PhD Program, Earth Science Department, University of Pisa, Via S. Maria 53, I-56126 Pisa, Italy

<sup>3</sup>Centre Tecnològic de Telecomunicacions de Catalunya (CTTC), Av. Carl Friedrich Gauss, 7, Castelldefels, Spain

<sup>4</sup>CNR, Consiglio Nazionale delle Ricerche, Istituto di Geoscienze e Georisorse, via G. La Pira 4, I-50121 Firenze, Italy

<sup>5</sup>Department of Physics and Astronomy, University of Bologna, Viale Berti-Pichat, 8, I-40127 Bologna, Italy

<sup>6</sup>ENEA, Italian National Agency for new Technologies, Energy and Sustainable Economic Development, via Martiri di Monte Sole, 4, I-40129 Bologna, Italy

Accepted 2016 June 10. Received 2016 May 18; in original form 2016 January 29

## SUMMARY

This work aims to explore the ongoing tectonic activity of structures in the outermost sector of the Northern Apennines, which represents the active leading edge of the thrust belt and is dominated by compressive deformation. We have applied the Persistent Scatterer Interferometry (PSI) technique to obtain new insights into the present-day deformation pattern of the frontal area of the Northern Apennine. PSI has proved to be effective in detecting surface deformation of wide regions involved in low tectonic movements. We used 34 Envisat images in descending geometry over the period of time between 2004 and 2010, performing about 300 interferometric pairs. The analysis of the velocity maps and of the PSI time-series has allowed to observe ground deformation over the sector of the Po Plain between Piacenza and Reggio Emilia. The time-series of permanent GPS stations located in the study area, validated the results of the PSI technique, showing a good correlation with the PS time-series. The PS analysis reveals the occurrence of a well-known subsidence area on the rear of the Ferrara arc, mostly connected to the exploitation of water resources. In some instances, the PS velocity pattern reveals ground uplift (with mean velocities ranging from 1 to 2.8 mm yr<sup>-1</sup>) above active thrust-related anticlines of the Emilia and Ferrara folds, and part of the Pede-Apennine margin. We hypothesize a correlation between the observed uplift deformation pattern and the growth of the thrust-related anticlines. As the uplift pattern corresponds to known geological features, it can be used to constrain the seismo-tectonic setting, and a working hypothesis may involve that the active Emilia and Ferrara thrust folds would be characterized by interseismic periods possibly dominated by aseismic creep.

**Key words:** Interferometry; Radar interferometry; Seismicity and tectonics; Continental tectonics: compressional; Dynamics: seismotectonics.

## 1 INTRODUCTION AND AIMS OF THE STUDY

This work aims to study the recent tectonic activity of the outermost structures of the Northern Apennines, namely the Pede-Apennine thrust front (PTF), which coincides with the morphological boundary between the Northern Apennines and the Po Plain. Lines of thrust folds are buried beneath the thick sedimentary infill of the Po Plain, which forms the shortened foreland of both the Northern Apennines and the Southern Alps. Since 1950s, the buried

compressional structures have been extensively explored through commercial seismic reflection lines and well logs for the petroleum industry.

This sector is characterized by historical and recent seismicity, with earthquake magnitude up to 6 (Rovida *et al.* 2011), such as for the 2012 Emilia seismic sequence that nucleated at the toe of the Apennine wedge (e.g. Pondrelli *et al.* 2012). Compressional strains are prevalent in the Po Plain, as shown by the fault plane solutions of instrumental earthquakes (e.g. Pondrelli *et al.* 2006; Scognamiglio *et al.* 2012), in agreement with geological and GPS evidence

(e.g. Devoti *et al.* 2011; Cenni *et al.* 2013). The strain rates are however rather low (Valensise & Pantosti 2001; Burrato *et al.* 2003; Basili *et al.* 2008; Maesano *et al.* 2015).

Assessing the seismic hazard of the external Northern Apennines is crucial due to the concentration of cities, infrastructures and industrial activities that occurs in this sector of the Emilia Romagna Region. In addition, the strong impact of human activity on this area has locally caused significant vertical ground motions (e.g. Stramondo *et al.* 2007; Bitelli *et al.* 2014), which complicates the understanding of the seismo-tectonic setting of the Northern Apennines margin.

Since 1990s, the Differential Synthetic Aperture Radar Interferometry (DInSAR) has been extensively used for active tectonic deformation assessment and it proved to be a powerful tool for providing detailed information about the nature of the deformation caused by the release of seismic energy (Massonnet *et al.* 1993; Massonnet & Feigl 1998; Price & Sandwell 1998; Lyons & Sandwell 2003; Wright *et al.* 2004). DInSAR technique measures the ground displacement in the line of sight (LOS), which is the slant vector between a pixel on the ground and the side-looking SAR sensor. The main limitations are related to the temporal and geometric decorrelation which causes a loss in coherence and prevents to derive measurements at every pixel position within the analysed area. The temporal decorrelation is caused by physical changes of the terrain or objects on the ground in the time span between the two acquisitions. The geometric decorrelation consists of variations in reflectivity of the targets, as a function of the incidence angle at the time of the SAR acquisitions (Zebker & Villasenor 1992; Hanssen 2001). In fact a drawback of the classical DInSAR techniques is the possible lack of coherence of the radar signal on vegetated areas and in different climatic conditions. An efficient solution to these problems has been provided by the multi-interferometric approaches grouped in the name of Persistent Scatterers Interferometry (PSI) techniques. These latter were exploited from the early 2000s to go beyond the conventional DInSAR methods by correcting for atmospheric, orbital and DEM (Digital Elevation Model) errors in order to obtain very accurate displacement and velocity measurements at specific points on the ground with millimetric precision (Ferretti *et al.* 2001, 2007; Werner *et al.* 2003; Crosetto *et al.* 2008). These techniques require a high number of satellite SAR data to provide mean deformation velocities and time-series of ground deformation over selected pointwise targets, the so-called PS or Persistent Scatterers (Ferretti *et al.* 2001). The PS are points which preserve the phase information in time and normally correspond to man-made objects (e.g. buildings) or single outcrops. PSI technique strongly minimize the loss of coherence between the acquisitions, but unfortunately limits the measurement points mainly to urbanized areas.

PSI has been widely applied for hydrogeological hazards investigations (Berardino *et al.* 2003; Hilley *et al.* 2004; Strozzi *et al.* 2005; Righini *et al.* 2012, Del Ventisette *et al.* 2014) and to reconstruct the history of deformations through PS time-series analysis (Bovenga *et al.* 2006; Colesanti & Wasowski 2006; Meisina *et al.* 2008; Righini *et al.* 2011). PSI has been also proved to be effective in detecting surface deformation of wide regions involved in low tectonic movements (where it is possible to find a considerable amount of PS) in various geodynamic environments, including orogenic fronts (Bürgmann *et al.* 2006; Massironi *et al.* 2009; Vilardo *et al.* 2009; Bell *et al.* 2011; Grandin *et al.* 2012; Béjar-Pizarro *et al.* 2013; Peyret *et al.* 2013). Besides to the original Permanent Scatterer technique (PSInSAR<sup>TM</sup>) patented by Ferretti *et al.* (2001), many different techniques have been developed to process multitemporal SAR data stacks such as the Small Baseline

Subset (SBAS) described by Berardino *et al.* (2002) and Lanari *et al.* (2004), the SqueeSAR method proposed by Ferretti *et al.* (2011) or other methods, see Costantini *et al.* (2000), Hooper *et al.* (2004), Kampes (2006) and Mora *et al.* (2003).

In this work, we applied the PS approach (PSIG procedure), implemented at the Geomatics Division of the Centre Tecnològic de Telecomunicacions de Catalunya (CTTC; Crosetto *et al.* 2011; Devanthéry *et al.* 2014), to obtain new insights into the present-day deformation pattern and anthropogenic subsidence of the sector between Piacenza and Reggio Emilia (Fig. 1). In this region, satellite interferometry techniques (DInSAR, SBAS and SqueeSAR<sup>TM</sup>) have been previously used to analyse the coseismic deformation of the 2012 Emilia seismic sequence (e.g. Bignami *et al.* 2012; Pezzo *et al.* 2013; Tizzani *et al.* 2013), as well as for studying the Po Plain subsidence (e.g. Strozzi *et al.* 2001; Stramondo *et al.* 2007; Bitelli *et al.* 2014; Pezzo *et al.* 2014). Finally, in order to validate the PSI measurements we compared our results with GPS data.

## 2 GEOLOGICAL SETTING AND MAIN ACTIVE STRUCTURES OF THE EXTERNAL NORTHERN APENNINES

The study area extends for about 100 km in northwest–southeast direction between Piacenza and Reggio Emilia, and comprises the Pede-Apennine margin and a wide part of the Po Plain (Fig. 1). The Po Plain is a syn-tectonic sedimentary wedge filling the Pliocene–Pleistocene Apenninic foredeep (Pieri & Groppi 1981; Cremonini & Ricci Lucchi 1982). The current geological setting of this area results from the activity of the outer thrusts in the foreland basin (Pieri & Groppi 1981; Boccaletti *et al.* 1985, 2004). The latter shows a monoclinical setting and corresponds to a large and undeformed structural element (Mariotti & Doglioni 2000). Along the Apennines–Po Plain margin, the outcropping rocks belong mainly to the Messinian evaporites and the post-evaporite succession (Tetto Formation, Colombacci Formation and Argille Azzurre Formation), sealed by the Pleistocene continental deposits of the Po Plain. The sedimentary sequence of the Po Plain consists of syn-tectonic deposits, with a general regressive trend that marks the transition from a marine to a continental environment (Ricci Lucchi *et al.* 1982). The continental sequence ends with the deposition of the Upper Emilia-Romagna Synthem (SERS, Reg. Emilia-Romagna 1998), which mainly consists of fluvial sediments (450 000 yr to present).

In the study area, three major systems of active structures can be distinguished, namely (i) the Pede-PTF, (ii) the Emilia folds and (iii) the Ferrara folds (Figs 1 and 2). The PTF separates the exposed portions of the Apennine wedge from the structures buried beneath the sediments of the Po Plain (Boccaletti *et al.* 1985; Toscani *et al.* 2009). This NE-verging thrust system is rather continuous and exhibits stacked thrust sheets (Pieri & Groppi 1981). However, the geomorphic surface expression of the PTF can be identified only in some zones, such as near Bologna and southwest of Reggio Emilia (Bonini 2007). Moderate to strong historical and recent earthquakes hit this sector (Fig. 3). Ongoing thrust activity is suggested by seismic data (Basili *et al.* 2008; DISS Working Group 2010), SAR interferometry (Stramondo *et al.* 2007), geomorphological analyses (Benedetti *et al.* 2003), as well as by the evolution of the erosional–depositional system along the Apennines foothills (Amorosi *et al.* 1996) and the displacement of Holocene terraces (Boccaletti *et al.* 2004, 2011; Gunderson *et al.* 2014). The presence of mud volcanoes along the Pede-Apennine foothills is indicative of



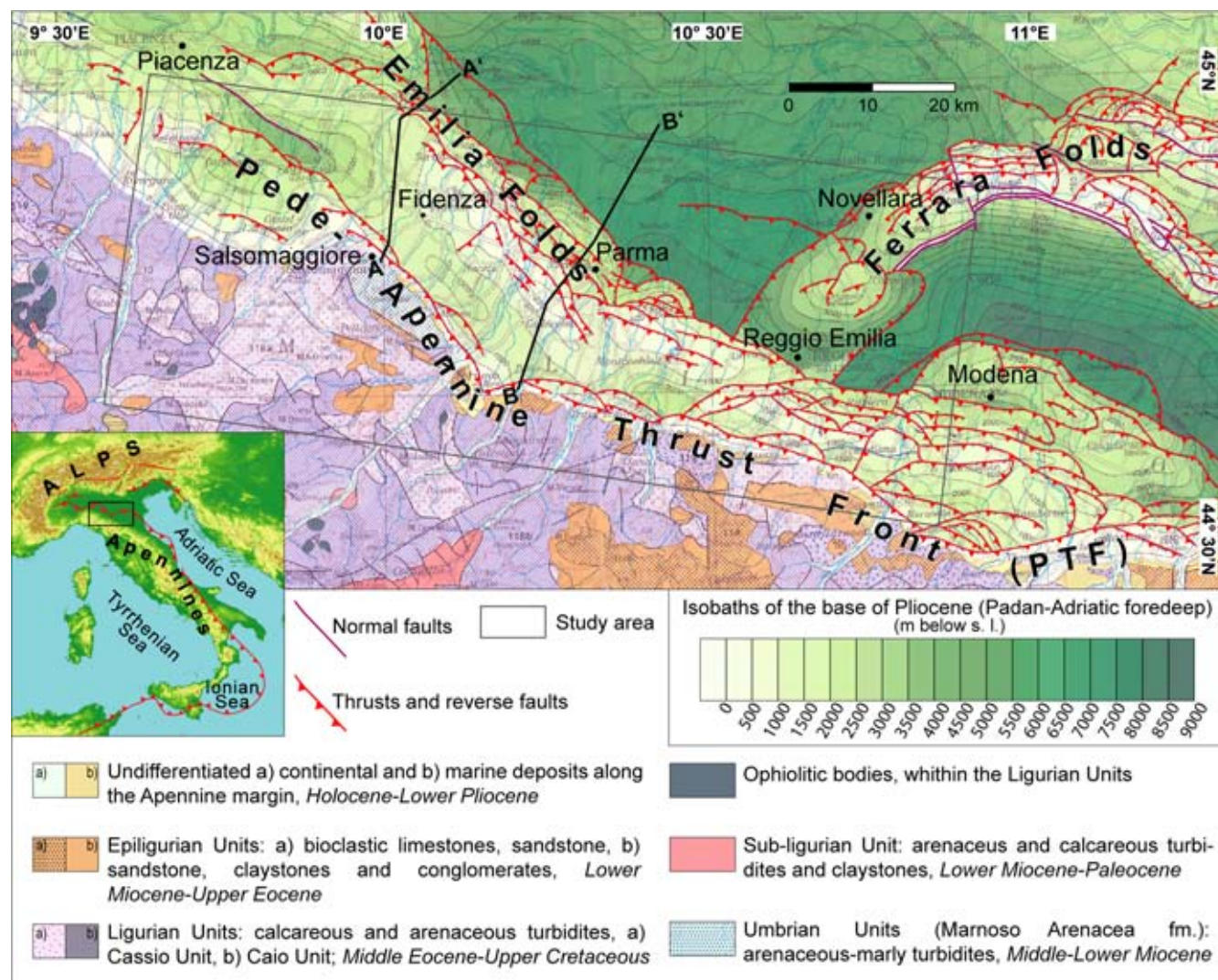


**Figure 1.** Structures and subsurface geology of the study area (grey box) (from Bigi *et al.* 1983).

large overpressures, which are essential for allowing the movement along the steeply dipping thrust faults composing the PTF (Bonini 2012).

The Emilia and the Ferrara folds systems are buried below the foredeep sediments (see cross-sections in Fig. 2), and include a series of thrusts and related folds that have a typical arcuate shape in map view (Fig. 1). The large sedimentation rate of the foredeep was accommodated by a considerable subsidence across the whole Po Plain, caused by the load of the Northern Apennines tectonic stack (e.g. Bartolini *et al.* 1996; Ghielmi *et al.* 2013). Tectonic subsidence rate was up to 2–3 mm yr<sup>-1</sup> (Arca & Beretta 1985; Carminati & Martinelli 2002; Stramondo *et al.* 2007; Cuffaro *et al.* 2010).

Historical and instrumental catalogues (Fig. 3; ISIDE Working Group 2010; Rovida *et al.* 2011) show that the seismicity concentrates along the buried thrust fronts (Emilia and the Ferrara folds). The earthquakes registered in the area in recent times are characterized by moderate seismicity and compressive/transpressive focal mechanism solutions (e.g. Pondrelli *et al.* 2006). The main recent seismic events in the area are the earthquakes of 1996 October 15 (Ciaccio & Chiarabba 2002) and 2012 May 20 and 29 (Pondrelli *et al.* 2012). Seismicity is not evenly distributed, but increases from

west to east, following the similar increase in the convergence rates across the whole Po Plain suggested by geodetic, seismological and tectonic evidences (D'Agostino *et al.* 2008; ISIDE Working Group 2010; Rovida *et al.* 2011; Maesano *et al.* 2015). In particular, the cumulative slip rate (calculated over the past 1.81 Ma) are ~0.70 mm yr<sup>-1</sup> and 0.95 mm yr<sup>-1</sup> for the Emilia and the Ferrara thrust front, respectively. Such an eastward increase in the strain rate (see also Boccaletti *et al.* 2011) matches the GPS observations, which document an increase of shortening from about 0.5 mm yr<sup>-1</sup> across the western Emilia thrust front to about 2.4 mm yr<sup>-1</sup> across the Ferrara thrust front (Michetti *et al.* 2012; Maesano *et al.* 2015) as well as the number of historical earthquakes and the released seismic moment (ISIDE Working Group 2010; Rovida *et al.* 2011; Burrato *et al.* 2012; Vannoli *et al.* 2015).

### 3 PSI TECHNIQUE: KEY ISSUES

The Persistent Scatterers Interferometry technique takes advantage of long temporal series of SAR data, acquired over the area of interest along the same satellite orbit, to filter out atmospheric artefacts and to identify points, that is, PSs, where high-precision measurements can be carried out. PSs are points on the ground (buildings,



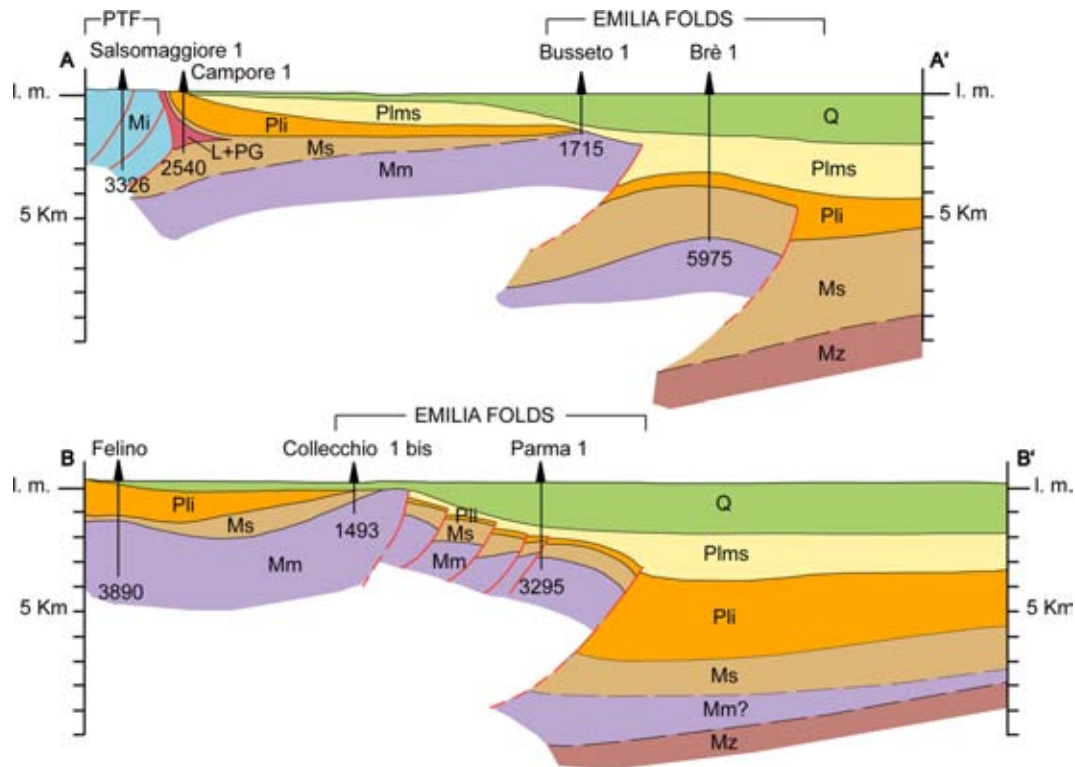


**Figure 2.** Transverse geological cross-sections of the external Northern Apennines (modified from Pieri & Groppi 1981). The traces of cross-sections are indicated in Fig. 1. Q: Quaternary; Plms: Upper Middle Pliocene; Pli: Lower Pliocene; Ms: Upper Miocene; Mm: Middle Miocene; Mi: Lower Miocene; PG: Paleogene; Mz: Mesozoic; L: Liguride.

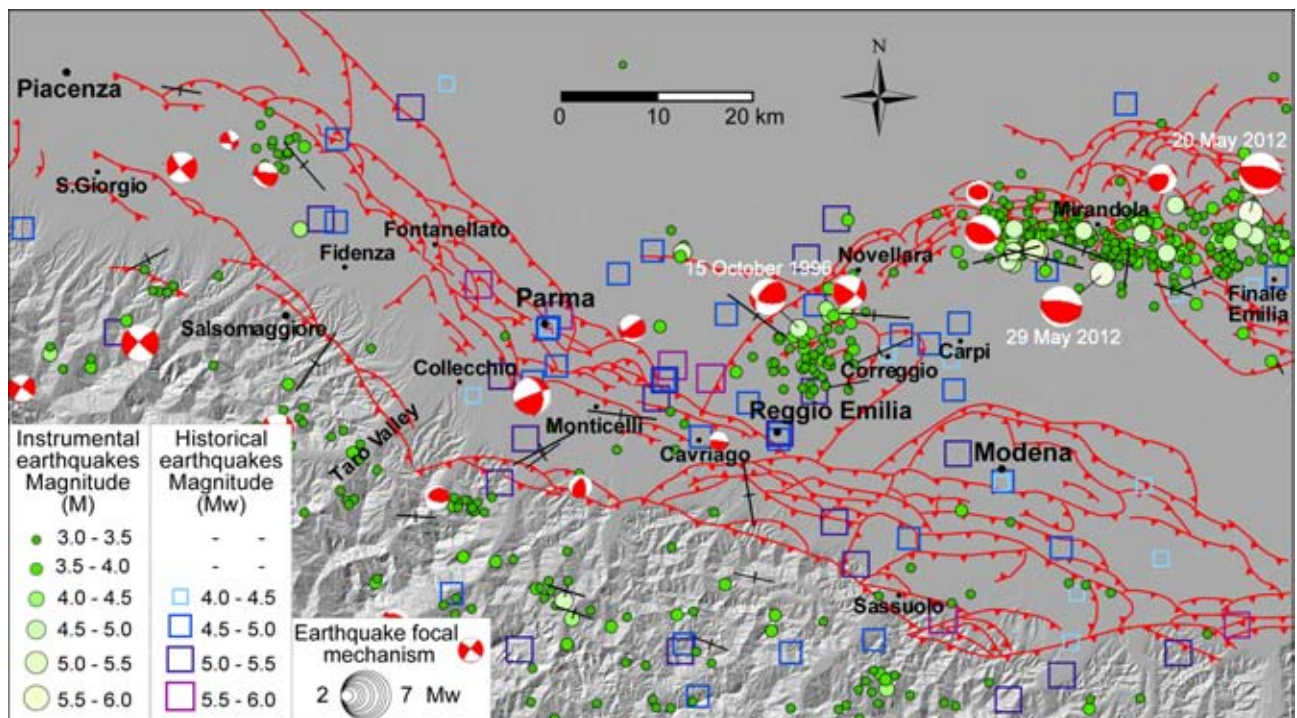


**Figure 3.** Seismotectonic map of the study area. The main structural elements are modified from the Structural Model of Italy (Bigi *et al.* 1983). Earthquake epicenters between 1985 and 2015, instrumentally recorded by the Istituto Nazionale di Geofisica are represented by green shades circles (ISIDe catalogue; <http://iside.rm.ingv.it>). The ISIDe catalogue contains instrumental earthquakes with different magnitude scales (i.e.  $M_d$ ,  $M_L$  and  $M_w$ ). Historical events ( $M_w$ ) are indicated by blue shades squares (CPTI11 catalogue, <http://emidius.mi.ingv.it/CPTI11/>; Rovida *et al.* 2011). Black crosses represent the orientation of the minimum horizontal stress ( $S_h$  min) deduced from breakout and focal mechanism analysis (Montone *et al.* 2012). Focal mechanisms are deduced from Regional Centroid Moment Tensor (RCMT, Pondrelli *et al.* 2006) and from the Quick RCMT online project of the Italian Istituto Nazionale di Geofisica e Vulcanologia (INGV) (available at: <http://autorcmr.bo.ingv.it/quicks.html>).

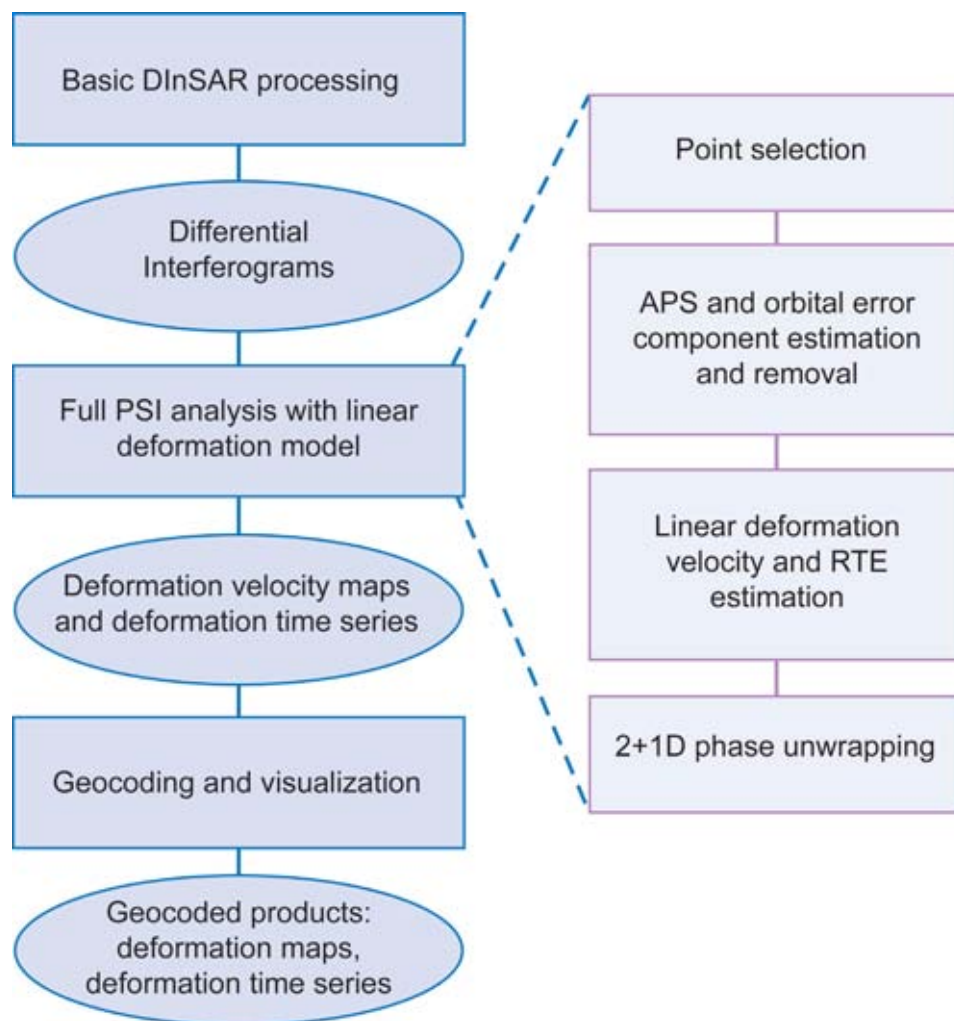


**Figure 4.** Flow chart representing the general scheme of the used PSI data analysis procedure.

rocks, etc.), which show a stable interferometric phase behaviour over time, that is, do not change their signature with time. PSs therefore can be used to estimate motion of the ground surface along the satellite LOS (about  $23^\circ$  tilted from the vertical axis for Envisat satellite). Very high PS densities are concentrated in urban environments, while low density occurs in agricultural landscape, vegetated area and in zones affected by foreshortening, layover and shadowing effects on the related SAR images. PS velocity values are relative to a reference point, chosen within the PS data set, which is considered stable. The precision of the resulting velocity estimates can range from 0.1 to 1 mm yr<sup>-1</sup> depending on the dispersion of amplitude (DA) of a specific PS pixel (Ferretti *et al.* 2007), as well as on the linearity of the movement that we are measuring, and decreases with distance from the reference point.

In this work, the PS approach implemented at the CTTC has been applied. The main steps of the procedure are shown in Fig. 4. Crosetto *et al.* (2011) provide a detailed description of the procedure. However, for sake of completeness, here below the key aspects of the applied approach for the particular case study of this work are briefly discussed. The starting point is a set of  $N$  single look complex SAR images from which a set of  $M$  interferograms is calculated ( $M \gg N$ ).

- **Point selection:** The point selection criterion is based on the DA. The DA index is a statistical parameter that evaluates the tem-

poral variability of the scatterer response for each point and can be used to evaluate the phase noise (Ferretti *et al.* 2001). The PS analysis was applied to points with DA lower than 0.3.

- **Atmospheric phase and orbital error components estimation and removal from the original interferograms:** This step consists in the estimation and removal of the APS (Atmospheric Phase Screen) contribution to the phase. It is performed by applying a sequence of spatial and temporal filters based on the assumption that the atmospheric component is characterized by smooth spatial phase gradients and a random behaviour in time. Moreover the PSI deformation velocity maps can be affected by tilts, which can be caused by uncompensated orbital errors, by the Envisat oscillator drift (Fattahi & Amelung 2014) and by the effect of the reference frame (Bähr *et al.* 2012), or uncompensated low-frequency atmospheric effects (e.g. see Bateson *et al.* 2010). These effects would result in a phase ramp, having a corresponding effect in the deformation time-series, and therefore they have been estimated and removed during the PSI analysis.

- **Linear deformation velocity and RTE estimation over the atmosphere free interferograms:** This step provides for each selected point three parameters: (i) the deformation velocity using a linear model of the deformation during the measured period and with respect to a reference point, (ii) the height of each measured PS with respect to the DEM used to calculate the network of differential interferograms (residual topographic error or RTE) and (iii) an

**Table 1.** List of the used Envisat descending images (spanning from 2004 September and 2010 September).

Number of images	Date of acquisition	Number of images	Date of acquisition
1	2004 September 30	18	2007 August 16
2	2004 November 4	19	2007 October 25
3	2004 December 9	20	2007 November 29
4	2005 January 13	21	2008 January 3
5	2005 February 17	22	2008 March 13
6	2005 April 28	23	2008 May 22
7	2005 July 7	24	2008 July 31
8	2005 September 15	25	2008 October 9
9	2005 November 24	26	2008 December 18
10	2006 February 2	27	2009 February 26
11	2006 April 13	28	2009 July 16
12	2006 June 22	29	2009 September 24
13	2006 August 31	30	2009 December 3
14	2006 November 9	31	2010 February 11
15	2007 January 18	32	2010 April 22
16	2007 March 29	33	2010 July 1
17	2007 June 7	34	2010 September 9

associated statistical parameter named temporal coherence ranging between 0 and 1 that evaluates the agreement between the observed interferometric phases (interferograms) and the linear deformation model. In this work, only the points with temporal coherence higher than 0.7 have been used. Although this rather high threshold can drive to a critical loose of measurements in areas affected by strong non-linear deformations, the authors consider that this is not a critical issue for this study, because we are interested mostly on linear deformation pattern. An in-depth description of the algorithm used to estimate the velocity and the RTE can be found in Biescas *et al.* (2007).

- **2 + 1D phase unwrapping:** In this step, the deformation time-series are derived. It consists in two steps: a 2-D phase unwrapping, performed interferogram wise which aims to solve the  $2\pi$  ambiguity (due to the fact that the interferometric phase is measured modulo  $2\pi$ ) adding the correct integer multiples of  $2\pi$ , and a temporal 1-D phase unwrapping. This procedure is described in detail in Monserrat (2012) and Devan  ry (2014). Note that in this step, the contribution of the RTE and the atmosphere has been removed from the original interferograms in order to derive the deformation measurements. The result of this step is, for each selected point, the temporal evolution of the phase along the measured period.

For our study, we selected 34 Envisat images in descending acquisition geometry (track 437 and frame 2709), spanning from 2004 September to 2010 September (Table 1). We computed a large number of all theoretically possible pairs (about 300 interferograms), setting a maximum threshold for the perpendicular baselines of 500 m. The major part of the topographic phase has been removed by using the 90-m pixel size SRTM DEM.

The procedure delivers two major outputs: the deformation velocity map that provides the deformation rates in millimetre per year for each measured PS, and the deformation time-series describing the PS behaviour during the measured period. Finally, we geocoded the data and represent the deformation velocity map by averaging pixels within an area of 100 m  $\times$  100 m. In Fig. 5, the number of PSs included in each pixel of 100 m  $\times$  100 m is shown.

## 4 DATA ANALYSIS

Fig. 6 shows the PSI linear deformation velocity map of ground movements of the PSs projected onto the satellite LOS. The reference area has been selected at Collecchio, where a GPS station (COLL) measured no significant deformation between 2007 and 2014. The reference area has been obtained averaging the PSs values within  $\sim 200$  m radius. The linear deformation velocity map is characterized by a high density of PSs in the cities and in the urban settlements, while PSs density gradually degrades outside. This can be explained by the frequent surface changes due to agricultural activities in the Po Plain, which affect the temporal correlation of the SAR signal.

The velocity map (Fig. 6) shows some clear patterns ascribable to different phenomena. The red zones (negative values) have moved away from the satellite and the blue parts of the map (positive values) indicate zone that moved toward the satellite. Although in principle every deformation acts in three dimensions (e.g. Samieie-Esfahany *et al.* 2010), we assume a mainly vertical deformation, given that the LOS is inclined at an angle close to the vertical and the horizontal displacements are significantly underestimated. This implies that the red zones are indicative of subsidence, while the blue zones indicate a relative ground uplift. Given the sensitivity of the sensor and the standard deviation analysis of the velocity values for the stable areas, the values of velocity between  $-1$  and  $1$  mm yr $^{-1}$  have been substantially considered as stable (green colour).

The time-series for each PS have been computed to estimate the temporal evolution of the deformation. In particular, the time-series show the relative LOS displacement of each PS relative to the first image. The analysis of the displacement time-series have also been useful for the comparison with GPS data (for a description of the time-series results, see the following Section 4.1).

### 4.1 PSI and GPS data comparison

Owing to the capability to detect millimetric displacements over long periods and large areas, advanced DInSAR techniques can be considered complementary to conventional techniques (levelling, GPS) for monitoring ground movements. Moreover, most of the PSI validation activities were based on the comparison of deformation velocities and time-series with estimations acquired by levelling or GPS measurements (Hanssen *et al.* 2008; Crosetto *et al.* 2016).

In particular, advanced DInSAR analyses make it possible to obtain very precise vertical displacement results on a dense network of measurements point, without installing any ground equipment. The integration of different methodologies have been widely employed to map land deformation in different contexts, such as tectonic assessment (e.g. B  rgmann *et al.* 2006; Wright *et al.* 2012; Peyret *et al.* 2013; Fuhrmann *et al.* 2015), volcanic activity (e.g. Pagli *et al.* 2006; Lagios *et al.* 2013) and subsidence phenomena (e.g. Zerbini *et al.* 2007; Bock *et al.* 2012; Caro Cuenca *et al.* 2012).

In order to improve the reliability of the outcomes shown in the previous paragraph, we compared the PSI results with those derived from the analysis of the permanent GPS stations that are present in the study area (Fig. 7). The GPS benchmarks occur at Parma (PARM) and Reggio Emilia (REGG) cities and in the Collecchio (COLL) and Gualtieri (RE01) towns (Fig. 8a; Baldi *et al.* 2009, 2011; Cenni *et al.* 2013).

The daily position time-series of these four sites have been estimated (together with several permanent stations located in the Italian peninsula and surrounding regions) with the method described in Cenni *et al.* (2013). The GPS time-series result from a series of



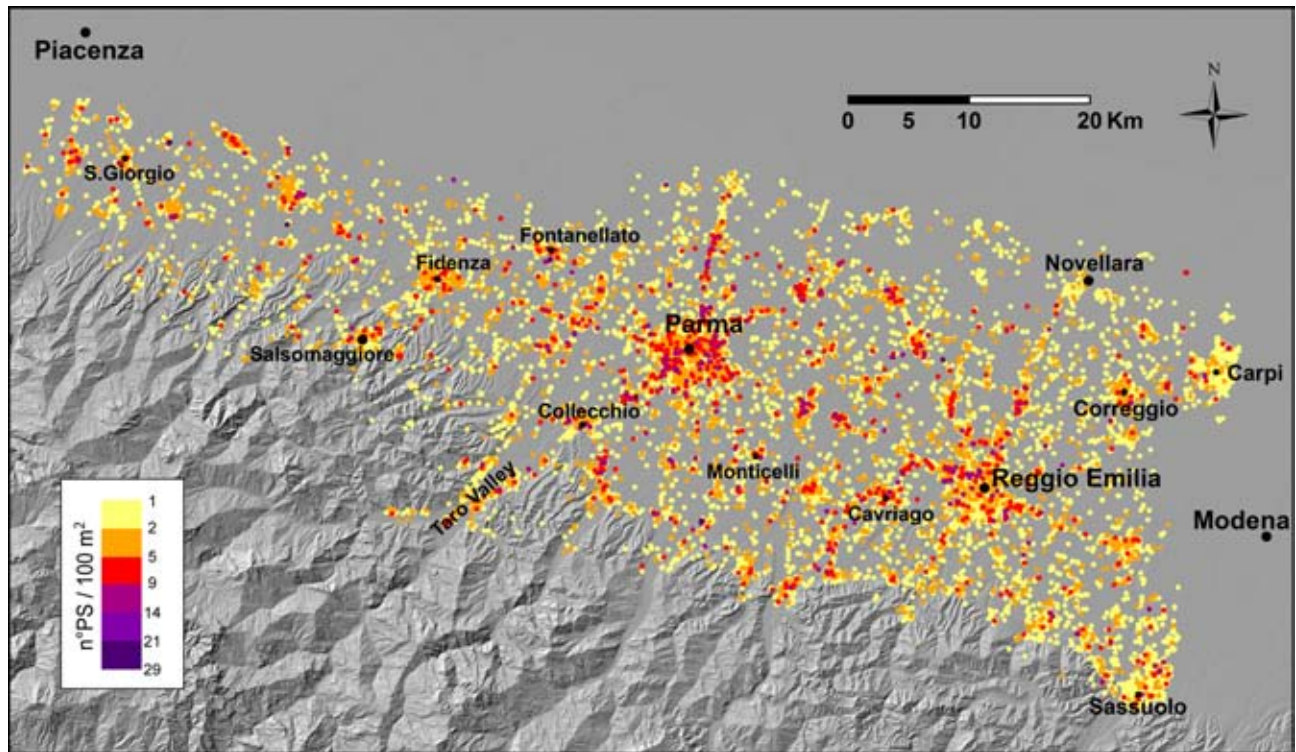


Figure 5. Number of PSs included in each pixel with a size of 100 m  $\times$  100 m.

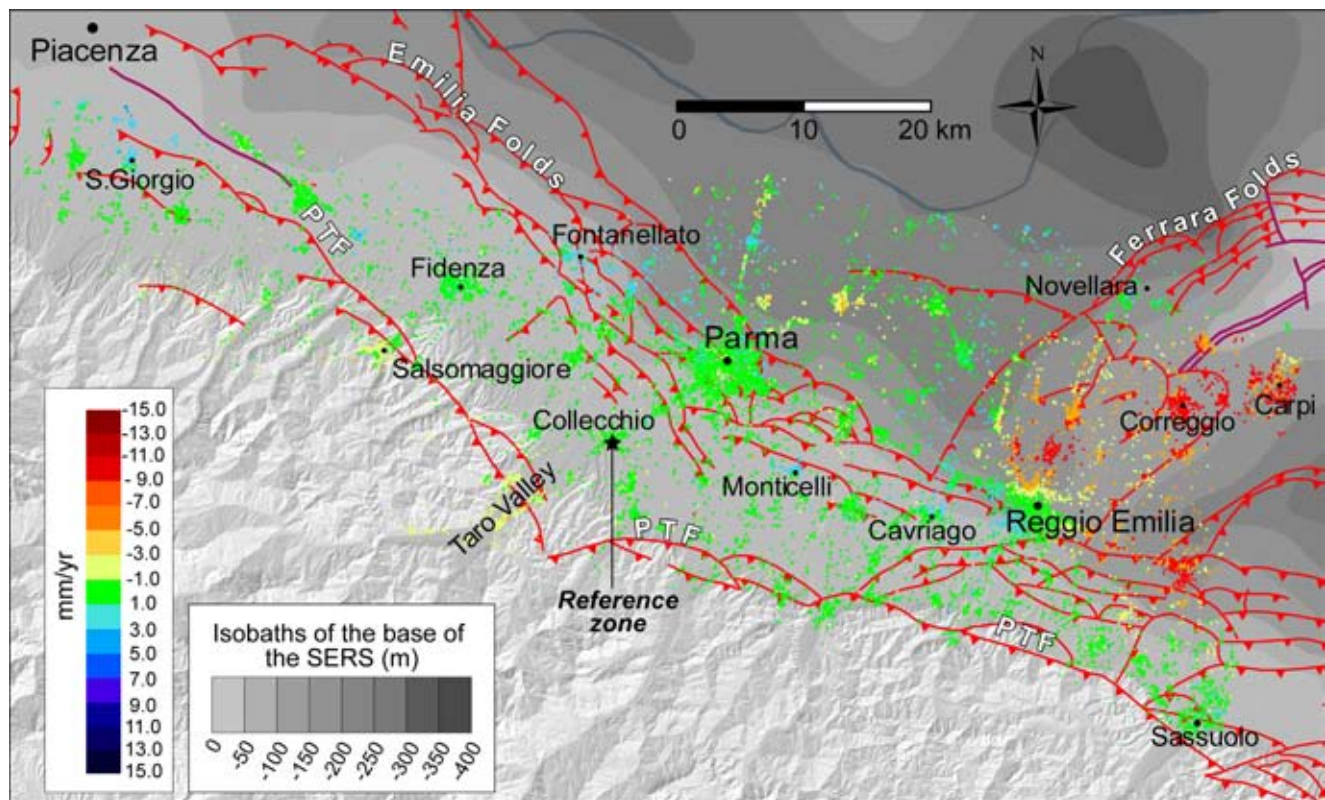
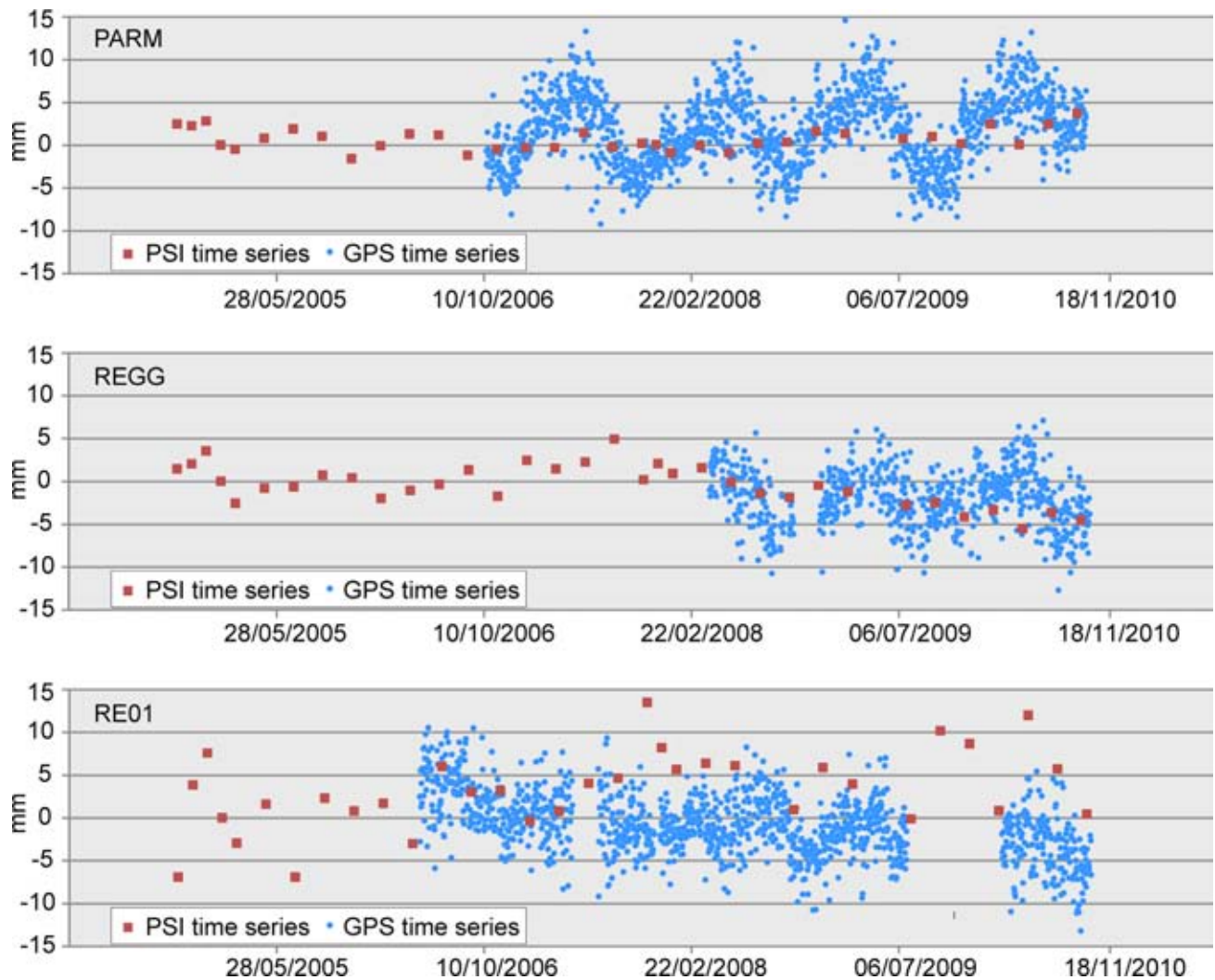


Figure 6. PS linear velocity map in the satellite LOS, from Envisat archives in descending orbit. The reference zone of the PSI linear deformation velocity is also shown (black star). The data have been plotted onto a shaded relief from a 10 m pixel Digital Terrain Model provided by the Regione Emilia-Romagna. Isobaths of SERS (Upper Emilia-Romagna Synthem) are modified from Boccaletti *et al.* (2004).



**Figure 7.** Comparison between the PSI and the GPS time-series (from 2004 September to 2010 September) projected along the satellite LOS, taking site COLL as reference.

coordinate components (north, east and vertical) of the site position, cleared up for outliers and steps due to instrument changing or/and earthquakes (see Cenni *et al.* 2012, 2013 for the processing details).

In order to compare the PSI time-series with the GPS ones, the latter have been projected along the Envisat LOS in descending geometry.

As stated earlier, owing to its roughly stable pattern, the area around site Collecchio (Cenni *et al.* 2012, 2013; COLL in Fig. 8a) has been chosen as reference area (supposed motionless) for the PSI data processing. In order to refer SAR and GPS at the same reference point, we subtracted the north, east and vertical components of site COLL from each of the remaining GPS stations included in the study area. Successively, we compared the LOS GPS time-series of these stations obtained through this procedure with those estimated from the PSI data (Fig. 7). The PSI time-series shown in Fig. 7 represent the average of the pixels closest to the GPS stations, within an area of  $200\text{ m} \times 200\text{ m}$  around the estimated position of the GPS receiver, as it may be difficult to identify a radar target in the same location of a GPS station. It is worth noting that the GPS time-series also contain a periodicity, which is not evident in the PSI time-series. This periodicity may be due to the characteristics of the substrate or to the characteristics of the mount of the GPS antenna. Periodic effects in GPS time-series may be related to temperature,

rain or atmospheric loading effects (Davis *et al.* 2012). Seasonal differences between winter and summer may, for instance, result in thermal expansion of the mount of the antenna.

The pattern of the GPS and PSI time-series are well comparable. Specifically, the PARM and the REGG time-series show a good agreement (Fig. 7). A lower correlation exists for the RE01 time-series (Fig. 7). The PSI time-series is rather noisy and may be influenced by some issues affecting the quality of the data: the RE01 station is indeed located on the edge of the frame, where the spatial filter used to remove the atmospheric error may not have correctly operated. Also, in this area the number of PSs is lower in comparison to the areas around the other GPS stations.

#### 4.2 PSI results overview and interpretation

In order to better observe the areas affected by ground deformation and to interpret the results, we have interpolated the velocity values to obtain an iso-kinematic map (Fig. 8a). In order to prevent extrapolation, the isolated (hence noisy) points have been excluded from the interpolation. Therefore, all the points over a distance  $> 1.5\text{ km}$  from the neighbouring point have been filtered. The iso-kinematic



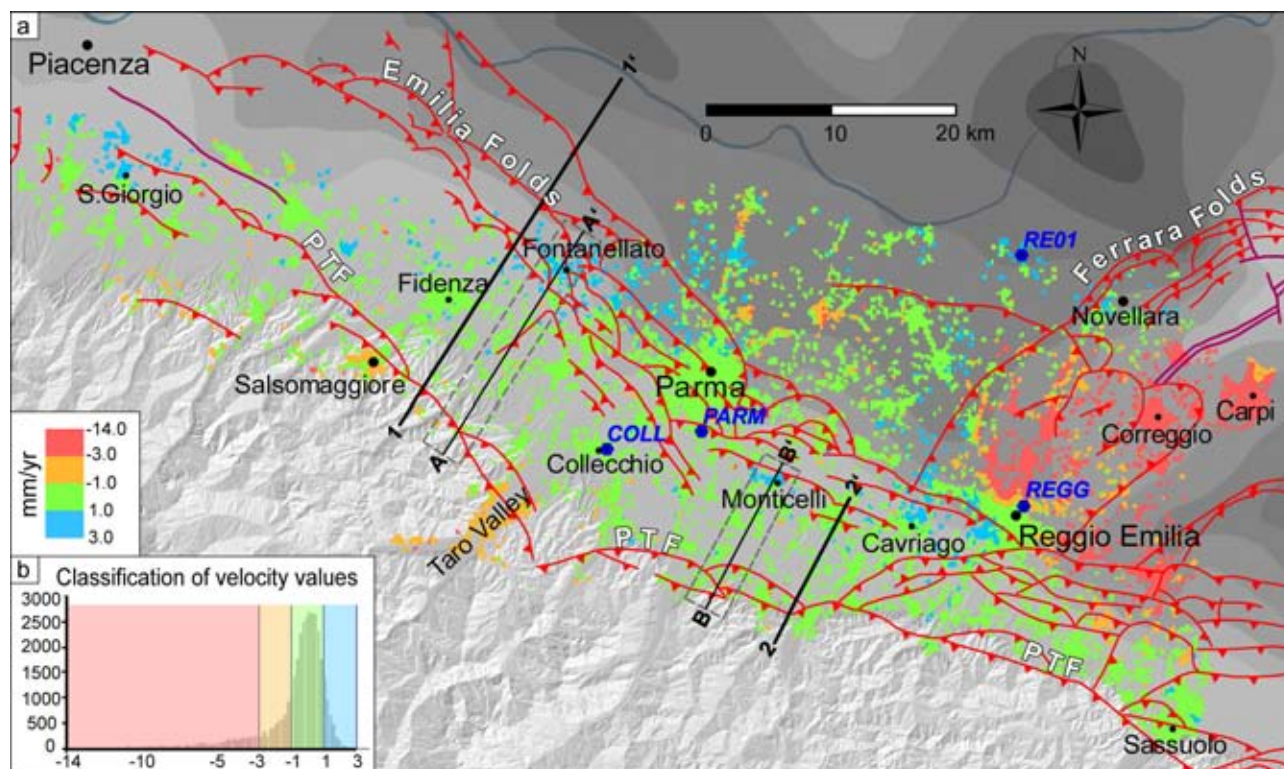


**Figure 8.** (a) Interpolated LOS linear deformation velocity map (Kriging method). The GPS stations RE01, COLL, REGG and PARM are indicated in blue; for SERS isobaths legend, see Fig. 6. The dashed boxes ( $\sim 3.3$  km wide) contain the velocity points used to build the LOS velocity profiles of Fig. 10. (b) Frequency histogram showing the statistical distribution of velocity values and the classification criterion of the PS velocity values.

map was derived in GIS environment by using the geostatistical Kriging technique. This interpolation method predicts the value at a given point by computing a weighted average of the known values in the neighbourhood of the unknown point. The weights used for the average depend on the spatial relationships between the measured values in the neighbourhood of the unknown point. We adopt a spherical semi-variogram model, with an interpolation search radius of 200 m, which has been chosen iteratively. The velocity values were subdivided into four classes to highlight the ground deformation patterns (see histogram in Fig. 8b). In order to interpret the possible causes of the observed ground deformation, the PSI results were compared with the geological, tectonic and seismological data available in literature.

We observe negative values of velocity that correspond to strong subsidence patterns in a wide area of the Po Plain, located in the eastern part of the study area, particularly around the cities of Reggio Emilia, Correggio and Carpi. The detected maximum subsidence rates are, respectively,  $-12$ ,  $-14$  and  $-13$  mm yr $^{-1}$ . The subsidence detected in the eastern part of the study area is a well-known phenomenon, which had already been highlighted by other studies (Strozzi *et al.* 2001; Carminati & Martinelli 2002; Stramondo *et al.* 2007; Baldi *et al.* 2009, 2011; Bock *et al.* 2012; Bitelli *et al.* 2014). The subsidence in the Po Plain is due to both natural and human-induced causes. Natural subsidence is the result of sediment compaction and loss of interstitial fluids produced by loading and tectonics. The detected amount of such displacement is of the order of  $2$ – $5$  mm yr $^{-1}$  in the area close to the piedmont Sabbiano anticline, nearby Bologna (Stramondo *et al.* 2007). The human-induced causes can be identified in the hydrocarbon and groundwater extraction, producing sediment compaction with at least one order of magnitude higher than that due solely to long-term natural processes

(Carminati & Martinelli 2002). Near Bologna, industrial and agricultural activities lead to a larger exploitation of water resources, and therefore the surface subsidence rates reaches  $40$ – $50$  mm yr $^{-1}$  (Stramondo *et al.* 2007). It is possible that a tectonic subsidence signal may also exist in the study area, but the remarkable negative velocity values ( $13$ – $14$  mm yr $^{-1}$  of subsidence) are dominantly attributable to the exploitation of water resource. More specifically, this pattern is mainly concentrated where the thickness of soft sediment is greater (i.e. at the towns of Correggio and Carpi) and the depth of the base of Pliocene increases (Figs 6 and 8a), particularly in correspondence of the large syncline south of the Ferrara arc (Fig. 1).

Our results were also compared with the vertical surface velocity map of the Po Plain sector of the Emilia Romagna Region for the period 2002–2006, created through the use of Envisat and Radarsat data (Bissoli *et al.* 2010; <http://www.arpa.emr.it/>) and with the updated regional subsidence map for the period between 2006 and 2011, obtained with the integrated use of continuous GPS stations and SqueeSAR<sup>TM</sup> analysis of Radarsat images (Bitelli *et al.* 2014). Both the shape of the areas subjected to subsidence, and the detected mean velocity values (e.g. from  $-12.5$  to  $-17$  mm yr $^{-1}$  of subsidence in the towns of Correggio and Carpi) are well comparable to our results (i.e.  $13$ – $14$  mm yr $^{-1}$  of subsidence).

A relative uplift pattern has been detected in several zones of the study area, where the deformation velocities are moderate and range from  $1$  to  $\sim 2.8$  mm yr $^{-1}$  (Fig. 8a). Interestingly, most of the uplift areas occur in correspondence of structures belonging to the main thrusts systems described above, particularly the PTF, the Emilia and the Ferrara folds. Given this spatial coincidence, we infer a correlation between the activity of some thrust-related anticlines buried below the Po Plain deposits and the surface deformation

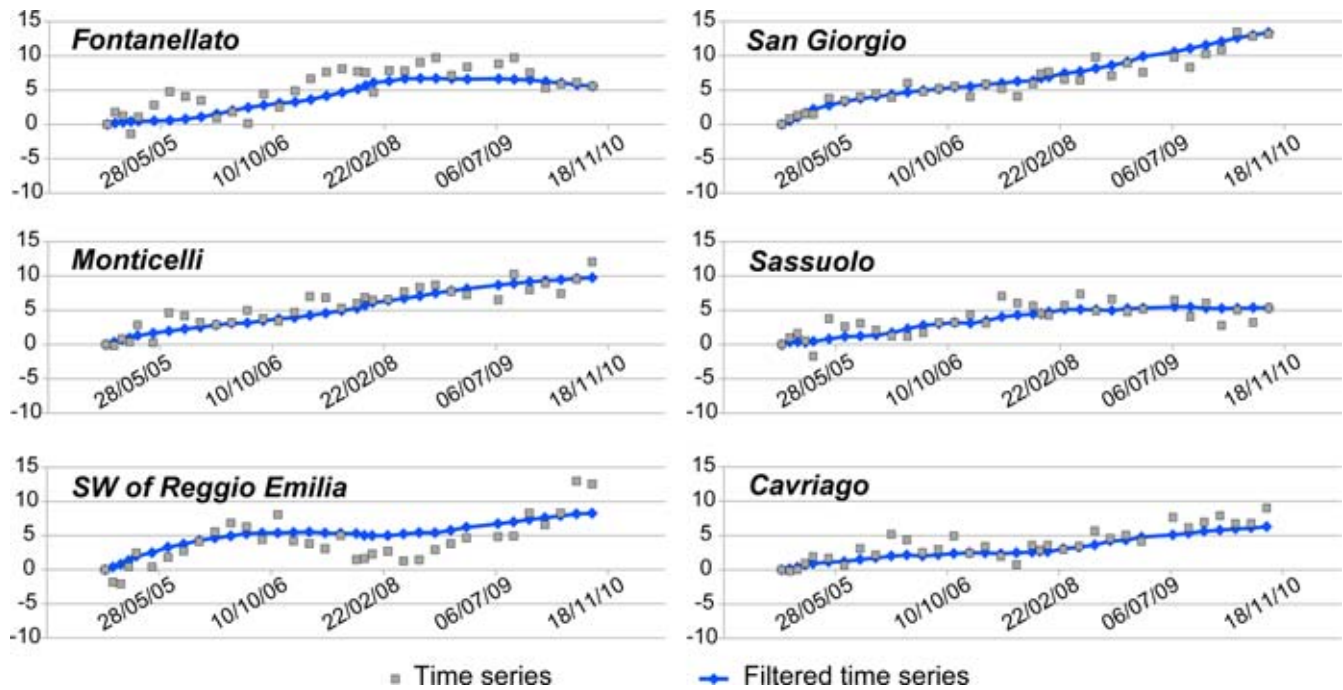


**Figure 9.** PSI time-series of the uplift zones in the analysed time span (from 2004 September to 2010 September). The filtered time-series are obtained through an average moving window with six samples.

pattern immediately above these structures (Fig. 8a). Pezzo *et al.* (2014) studied a wide area in the Po Plain through the use of ERS, Envisat and COSMO-SkyMed images processed with the SBAS technique. Importantly, they observed a rough correspondence between the growth anticline and the positive velocity values. Our study area overlaps with the velocity map of Pezzo *et al.* (2014) between Parma and Reggio Emilia, and we find a good agreement for most of the observed ground deformation. In addition, most of the uplifting areas over the Emilia folds detected in this study have been also reported as local zones of tectonic uplift in the geomorphological map of Castiglioni *et al.* (1997).

Fig. 9 shows the time-series of the uplift zones, representing the LOS motion component of PSs as a function of time. The time-series were calculated as an average of the four pixels centred in each zone of uplift (i.e. the time-series were averaged on an area of  $200 \text{ m} \times 200 \text{ m}$ ) in order to represent the general deformation pattern of each uplift zones. Most of the time-series have an approximately linear trend with constant angle of slope (that represents the mean velocity value), indicating a roughly constant movement towards the satellite during the six years of measurements. Such patterns may represent a relatively slow tectonic movement, although other movements involving the superficial layers of the subsoil may superimpose on the tectonic signal. Specifically, the cessation or a significant reduction of water pumping (e.g. Gambolati & Teatini 2015) could be invoked to explain the origin of the ground uplift movement in the surveyed areas. The uplift induced by the groundwater recovery after long-term intensive pumping originated from relaxation of elastically compressed aquifer materials (elastic rebound; Allen & Mayuga 1969; Waltham 2002; Martín *et al.* 2014) has been monitored through InSAR technique (Schmidt & Bürgmann 2003; Bell *et al.* 2008). This phenomenon is characterized by a transition from subsidence to uplift (Chen *et al.* 2007), as reported in Venice, Italy (e.g. Gatto & Carbognin 1981). This specific trend is not present in the time-series (Fig. 9), nor it is reported in literature for the study area, and thus we have no evidence to support this hypothesis.

Another anthropogenic factor that may cause ground uplift may be related to underground gas storage. The storage of natural gas can be realized in depleted gas fields, which are present in the investigation area. However, the concession areas of storage shown in the map of the mineral rights in force of the Emilia Romagna (downloaded at <http://unmig.sviluppoeconomico.gov.it/unmig/cartografia/cartografia.asp>; updated to 2013 August 31) do not correspond to those affected by uplift, and therefore this possibility can be ruled out.

The zones affected by uplift are described below by reference to the main thrusts systems:

- *Pede-Apennine thrust front:* The surface deformation pattern of the morphological boundary between the Apennine and the Po Plain is characterized by a stable setting during the investigated time span (2004–2010). There are however some important exceptions, particularly the town of S. Giorgio Piacentino, in the westernmost part of the study area, is characterized by an uplift pattern covering an area of  $\sim 30 \text{ km}^2$ , reaching a maximum velocity of about  $2.8 \text{ mm yr}^{-1}$  (Figs 6 and 8a). These uplift values are in agreement with the vertical surface velocity map of Bitelli *et al.* (2014), which indicate for this area values between  $2.5$  and  $5 \text{ mm yr}^{-1}$ . As shown in Figs 6 and 8(a), the ‘S. Giorgio Piacentino uplift zone’ is located over the hangingwall of a thrust fault. Moderate negative velocity values (mean of about  $-2 \text{ mm yr}^{-1}$ ) are instead detected at the Taro Valley and around Salsomaggiore. This pattern may be related to a deformation (pumping-induced subsidence due to the compaction of the river sediments) or rather to a residual atmospheric disturbance due to the particular location of this zone, which is between the hilly region and the plain, at the border of the study area. Owing to these conditions, the spatial filter used to remove the atmosphere component might have not worked correctly, therefore we have not enough information to discard the presence of an atmosphere disturbance.

- *Emilia folds:* A relatively large area (approximately  $45 \text{ km}^2$ ) of the Po Plain between Parma and Fidenza shows an uplift pattern



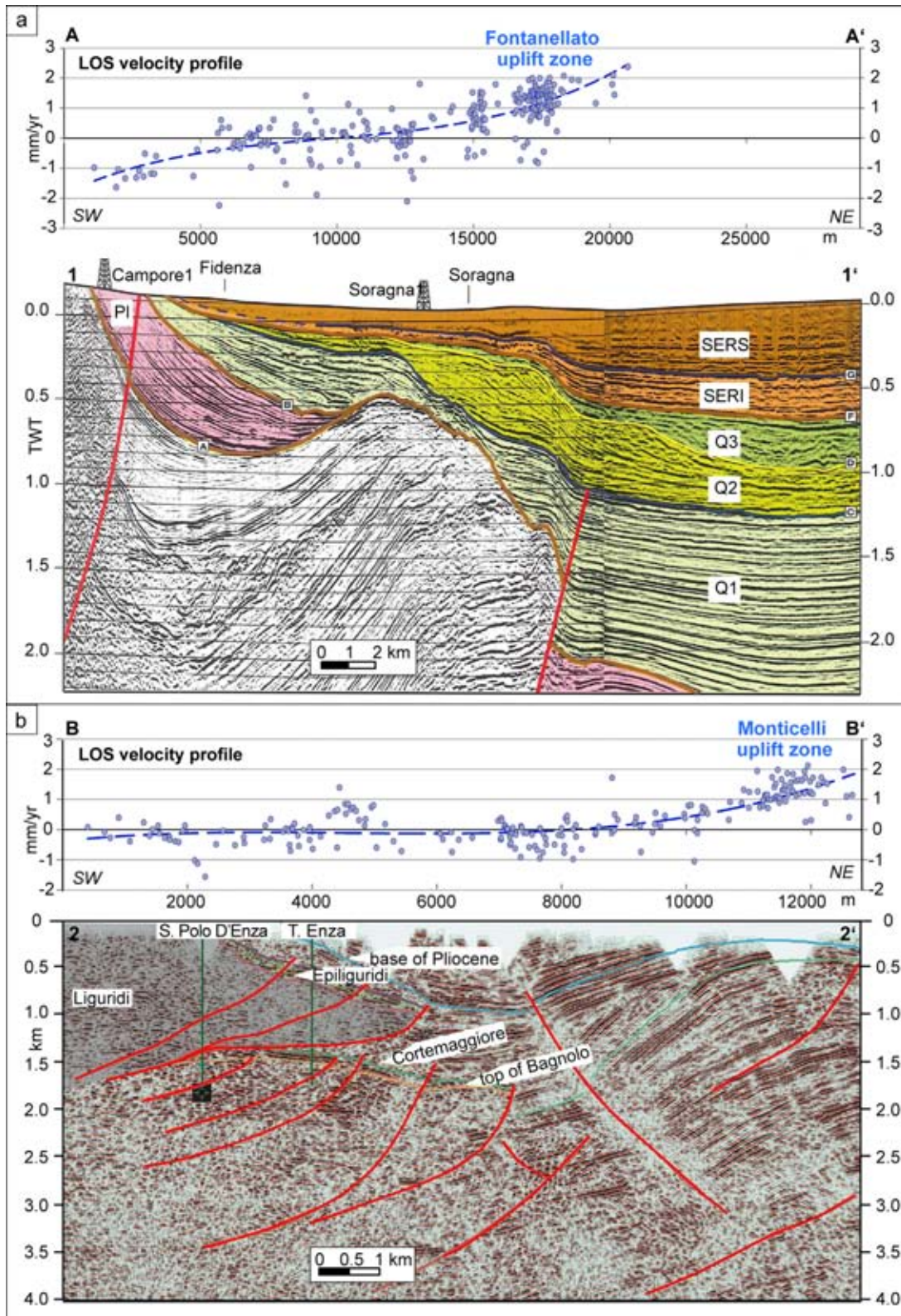


**Figure 10.** Comparison between the LOS velocity profiles of the uplift zones and the interpreted seismic sections located near the uplift zones. The LOS velocity profiles are represented with a distribution of velocity points that are contained in strips parallel to the cross-sections (dashed boxes in Fig. 8a). The best fit of point distribution is represented by a polynomial regression lines of order three. For the location of the velocity profiles and the seismic sections see Fig. 8(a). (a) 'Fontanellato uplift zone'. A–A': LOS velocity profile; 1–1': seismic section; SERS: Upper Emilia-Romagna Synthem, SERI: Lower Emilia-Romagna Synthem, Q1, Q2 and Q3: Quaternary Marine Sequence (after Reg. Emilia-Romagna 1998). (b) 'Monticelli uplift zone'. B–B': LOS velocity profiles; 2–2': seismic section (interpreted seismic line PR-314-80v, Progetto ViDEPI, [http://unmig.sviluppoeconomico.gov.it/videpi/cessati/sismica\\_titoli.asp](http://unmig.sviluppoeconomico.gov.it/videpi/cessati/sismica_titoli.asp)).

that ranges from 1.3 to 2 mm yr<sup>-1</sup> (Figs 6 and 8a). This area also includes the small village of Fontanellato and is here referred to as 'Fontanellato uplift zone'. Several thrust faults in this area form a morphological high (Bigi *et al.* 1983) and some faults are considered to be active (Boccaletti *et al.* 2004, 2011). This sector is however essentially devoid of instrumentally recorded earthquakes, while it was hit by the historical earthquake of 1438 ( $M_w \approx 5.6$ , Guidoboni *et al.* 2007) (Fig. 3). These faults affect the sedimentary succession up to the most recent levels, as illustrated in the interpreted seismic profile 1–1' (Fig. 10a), in which the SERS reflectors are clearly deformed.

Cross-section A–A' in Fig. 10(a) represents an LOS velocity profile traced parallel to the seismic section 1–1'. The velocity profile has been projected onto the seismic line (about 3 km to the west) along the structural strike, that is, the mean trend of the thrust faults. The underground structural setting in correspondence of the velocity profile is supposed to look similar to the seismic section. The velocity profile A–A' across the 'Fontanellato uplift zone' is shown by plotting all the measuring points lying inside a 3.3-km-wide strip (dashed box in Fig. 8a), parallel to cross-section A–A'. The comparison between the LOS and the seismic profiles shows that the 'Fontanellato uplift zone' coincides with the crest of the buried thrust anticline (Fig. 10a).

The Monticelli village and surrounding areas (Figs 6 and 8a) are affected by uplift from 1.6 to 2 mm yr<sup>-1</sup>. This zone is clearly located at the top of a thrust anticline that represents a morphological high of the substrate, such that the Quaternary sediments are here only 10 m thick (Petrucchi *et al.* 1975; Calda *et al.* 2007). The Monticelli anticline is connected with an active thrust fault (Boccaletti *et al.* 2004), and is well imaged along a seismic reflection profile 2–2' (Fig. 10b). In particular, the Monticelli uplift zone occurs over the same thrust imaged in the seismic line 2–2', which is situated almost 5 km to the east. Cross-section B–B' in Fig. 10b (obtained using the same procedure as for section A–A') illustrates an LOS velocity profile along a transect crossing the Monticelli anticline, and parallel to the seismic section 2–2'. The comparison between the LOS profile and the seismic section shows that the 'Monticelli uplift zone' corresponds to the crest of the thrust-related anticline (Fig. 10b).

An uplift zone of ~30 km<sup>2</sup> occurs east–southeast approximately along the same structure near Cavriago and in the southwestern part of Reggio Emilia city. In this sector, ground uplift ranges from 1 to 1.8 mm yr<sup>-1</sup>, and occurs over an area close to a NW–SE trending thrust system. A number of historical earthquakes struck the Reggio Emilia city, the largest of which was the  $M_w = 5.14$  of 1547 (Fig. 3; Guidoboni *et al.* 2007). It is possible that the structures producing the current uplift are the same that originated the historical earthquakes. Finally, a moderate uplift signal affects the northwestern part of Parma.

- *Ferrara folds:* Although the area of study comprises only the western part of the Ferrara arc, it is worth noting that some signals of uplift (up to 1.5 mm yr<sup>-1</sup>) occur in correspondence to the arcuate-shaped main thrust front at the town of Novellara. Several instrumental and historical earthquakes are reported in this zone (Fig. 3), and together with geomorphic data mentioned in the previous paragraphs (Castiglioni *et al.* 1997; Burrato *et al.* 2003; Scrocca *et al.* 2007; Boccaletti *et al.* 2011), indicate that this structure is potentially seismogenic.

To summarize, the PSI results reveal that some buried thrust anticlines along the Pedo-Apennine margin and Po Plain are

characterized by surface uplift. In these structural settings, ground uplift is often taken as evidence for ongoing tectonic activity (e.g. Massironi *et al.* 2009; Champenois *et al.* 2012; Grandin *et al.* 2012; Perrone *et al.* 2013; Peyret *et al.* 2013). This interpretation is in good agreement with the geological, seismological and morphological evidence supporting the activity of these structures (e.g. Benedetti *et al.* 2003; Burrato *et al.* 2003; Boccaletti *et al.* 2004, 2011; Basili *et al.* 2008). The areas of surface uplift are also characterized by historical and current seismic activity. In particular, the macroseismic epicentre of several historical earthquakes are localized along the Emilia folds, and partly along the Ferrara folds. The instrumental earthquakes are instead rather infrequent along the Emilia folds, whereas the Ferrara folds show large clusters that followed the main seismic events of 1996 October and 2012 May. On the basis of these observations, a working hypothesis may involve that the active Emilia and Ferrara thrust folds would be characterized by interseismic periods basically dominated by aseismic creep. The analysis of the 2012 seismic sequence apparently corroborates this possibility, in that the area above the thrust fault rupture was uplifting before the earthquake, but it was essentially devoid of previous instrumental events. In particular, the analysis of the deformation maps of Pezzo *et al.* (2014) and of Bitelli *et al.* (2014) reveals that the areas above the thrust faults that ruptured on 2012 May 20 and 29 (just outside our area of study) were slightly uplifting in the period 1992–2010, prior to the earthquakes. Cenni *et al.* (2013, 2014) identified minor uplift of the order of ~0.5 mm yr<sup>-1</sup> in the zone of Mirandola through GPS data, for the period 2001 January 1–2012 April 30. Also the GPS vertical velocities map of Devoti *et al.* (2011) indicate minor positive values for this area. On this basis, a preliminary interpretation of the 2012 earthquake sequence would be that fault rupturing was preceded by aseismic uplift. The lessons from the latter case may suggest that the nowadays uplifting thrust folds discussed in this study may exhibit a similar behaviour, even though we cannot establish whether these will accommodate deformation through aseismic creep or through episodic earthquakes. A further possibility that we should take into account to explain the aseismic ground uplift above anticlines would be connected to fold amplification mechanisms (e.g. fault-propagation folding).

## 5 CONCLUSIONS

The Pedo-Apennine margin of the Northern Apennines and the southern part of the Po Plain are tectonically active areas. This work has attempted to correlate the superficial deformation signals measured by radar satellite-based sensor with the known geological features. On the basis of the analysis of both the linear deformation velocity maps and the PSI time-series, the ground deformation has been analysed over a wide sector of the Po Plain, specifically between Piacenza and Reggio Emilia. The PS analysis reveals an important subsidence area, which is primarily linked to the exploitation of water resources. The areas subjected to the maximum velocities of subsidence approximately coincide with a large synform south of the Ferrara arc, where the sedimentary package is thicker. The results also revealed some areas of relative ground uplift with velocities ranging between 1 and 2.8 mm yr<sup>-1</sup>. The uplift deformation zones are mostly located in correspondence of the belts of subsurface active thrust folds, and thus we hypothesize a correlation between the observed uplift deformation pattern and the growth of the thrust-related anticlines. As the uplift pattern corresponds to known geological features, it can be used to constrain the seismo-tectonic setting. However, ground uplift has been detected in



correspondence of only a number of active thrust folds. Since thrust fold activity is likely to be episodic, the short time span of analysis may allow to capture only a part of the ongoing deformation. The ongoing uplift identified for some thrust folds does not imply that this will necessarily lead to an earthquake, yet the results of the current analysis should be taken into proper account when evaluating the seismic hazard of the study region. In this regard, Sentinel-1 satellites will provide new high-quality data (i.e. improved SAR data availability, larger coverage and shorter temporal sampling) for developing and testing models of the earthquake preparation processes, which will generate a strong increase in the observation of crustal deformation worldwide (e.g. Tolomei *et al.* 2015).

## ACKNOWLEDGEMENTS

Satellite radar data are provided by the European Space Agency (ESA Category 1 Project 13866). We thank María Cuevas-González and Dario Delle Donne for the helpful comments and the evaluable technical support. We thank the anonymous reviewers for the several constructive comments.

## REFERENCES

- Allen, D.R. & Mayuga, M.N., 1969. The mechanics of compaction and rebound, Wilmington Oil Field, Long Beach, California, U.S.A., in *Proceedings of the Tokyo Symposium on Land Subsidence*, Vol. 2, pp. 410–423, International Association of Scientific Hydrology and UNESCO, Tokyo.
- Amorosi, A., Farina, M., Severi, P., Preti, D., Caporale, L. & Di Dio, G., 1996. Genetically related alluvial deposits across active fault zones: an example of alluvial fan-terrace correlation from the upper Quaternary of the southern Po Basin, Italy, *Sediment. Geol.*, **102**, 275–295.
- Arca, S. & Beretta, G.P., 1985. Prima sintesi geodetico-geologica sui movimenti verticali del suolo nell'Italia Settentrionale (1897–1957), *Boll. Geod. Sc. Aff.*, **44**, 125–156.
- Bähr, H., Samiei-Esfahany, S. & Hanssen, R.F., 2012. On the effect of reference frame motion on InSAR deformation estimates, in *Proceedings of Fringe 2011 Workshop*, Vol. SP-697, ed. Ouwehand, L., 19–23 September 2011, ESA Publications, Frascati, Italy.
- Baldi, P., Casula, G., Cenni, N., Loddo, F. & Pesci, A., 2009. GPS-based monitoring of land subsidence in the Po Plain (Northern Italy), *Earth planet. Sci. Lett.*, **288**, 204–212.
- Baldi, P., Casula, G., Cenni, N., Loddo, F., Pesci, A. & Bacchetti, M., 2011. Vertical and horizontal crustal movements in central and northern Italy, *Boll. Geof. Teor. Appl.*, **52**(4), 667–685.
- Bartolini, C., Caputo, R. & Pieri, M., 1996. Pliocene–quaternary sedimentation in the Northern Apennine foredeep and related denudation, *Geol. Mag.*, **133**(3), 255–273.
- Basili, R., Valensise, G., Vannoli, P., Burrato, P., Fracassi, U., Mariano, S., Tiberti, M.M. & Boschi, E., 2008. The Database of Individual Seismogenic Sources (DISS), version 3: summarizing 20 years of research on Italy's earthquake geology, *Tectonophysics*, **453**, 20–43.
- Bateson, L., Novali, F. & Cooksley, G., 2010. TerraFirma user guide: a guide to the use and understanding of Persistent Scatterer Interferometry in the detection and monitoring of terrain-motion, TerraFirma project, ESRIN/Contract no. 19366/05/I-E, <http://www.terrafirma.eu.com/users.htm>.
- Béjar-Pizarro, M., Socquet, A., Armijo, R., Carrizo, D., Genrich, J. & Simons, M., 2013. Andean structural control on interseismic coupling in the North Chile subduction zone, *Nat. Geosci. Lett.*, **6**, 462–467.
- Bell, J.W., Amelung, F., Ferretti, A., Bianchi, M. & Novali, F., 2008. Permanent scatterer InSAR reveals seasonal and long-term aquifer system response to groundwater pumping and artificial recharge, *Water Resour. Res.*, **44**, W02407, doi:10.1029/2007WR006152.
- Bell, A.F., Naylor, M., Heap, M.J. & Main, I.G., 2011. Forecasting volcanic eruptions and other material failure phenomena: an evaluation of the failure forecast method, *Geophys. Res. Lett.*, **38**, L15304, doi:10.1029/2011GL048155.
- Benedetti, L., Tapponnier, P., Gaudemer, Y., Manighetti, I. & Van der Woerd, J., 2003. Geomorphic evidence for an emergent active thrust along the edge of the Po Plain: the Broni-Stradella fault, *J. geophys. Res.*, **108**(B5), 2238, doi:10.1029/2001JB001546.
- Berardino, P., Fornaro, G., Lanari, R. & Sansosti, E., 2002. A new algorithm for surface deformation monitoring based on small baseline differential SAR interferograms, *IEEE Trans. Geosci. Remote Sens.*, **40**, 2375–2383.
- Berardino, P., Costantini, M., Franceschetti, G., Iodice, A., Pietranera, L. & Rizzo, V., 2003. Use of differential SAR interferometry in monitoring and modelling large slope instability at Maratea (Basilicata, Italy), *Eng. Geol.*, **68**(1–2), 31–51.
- Biescas, E., Crosetto, M., Agudo, M., Monserrat, O. & Crippa, B., 2007. Two radar interferometric approaches to monitor slow and fast land deformations, *J. Surv. Eng.*, **133**, 66–71.
- Bigi, G. *et al.*, 1983. *Structural Model of Italy 1:500 000*, CNR Progetto Finalizzato Geodinamica.
- Bignami, C. *et al.*, 2012. Coseismic deformation pattern of the Emilia 2012 seismic sequence imaged by Radarsat-1 interferometry, *Ann. Geophys.*, **55**(4), 2012, doi:10.4401/ag-6157.
- Bissoli, R., Bitelli, G., Bonsignore, F., Rapino, A. & Vittuari, L., 2010. Land subsidence in Emilia-Romagna Region, northern Italy: recent results, in *Land Subsidence, Associated Hazards and the Role of Natural Resources Development*, Vol. 339, pp. 307–311, IAHS Publications.
- Bitelli, G., Bonsignore, F., Del Conte, S., Novali, F., Pellegrino, I. & Vittuari, L., 2014. Integrated use of advanced InSAR and GPS data for subsidence monitoring, in *Proceedings of IAEG XII Congress*, Torino, September 15–19, pp. 147–150.
- Boccaletti, M. *et al.*, 1985. Considerations on the seismotectonics of the Northern Apennines, *Tectonophysics*, **117**, 7–38.
- Boccaletti, M. *et al.*, 2004. *Carta Sismotettonica Della Regione Emilia-Romagna, Scala 1:250 000*, S.El.Ca., Firenze, 2004.
- Boccaletti, M., Corti, G. & Martelli, L., 2011. Recent and active tectonics of the external zone of the Northern Apennines (Italy), *Int. J. Earth Sci.*, **100**, 1331–1348.
- Bock, Y., Wdowinski, S., Ferretti, A., Novali, F. & Fumagalli, A., 2012. Recent subsidence of the Venice Lagoon from continuous GPS and interferometric synthetic aperture radar, *Geochem. Geophys. Res. Lett.*, **13**(3), doi:10.1029/2011GC003976.
- Bonini, M., 2007. Interrelations of mud volcanism, fluid venting, and thrust-anticline folding: examples from the external northern Apennines (Emilia-Romagna, Italy), *J. geophys. Res.*, **112**, B08413, doi:10.1029/2006JB004859.
- Bonini, M., 2012. Mud volcanoes: indicators of stress orientation and tectonic controls, *Earth Sci. Rev.*, **115**, 121–152.
- Bovenga, F., Nutricato, R., Refice, A. & Wasowski, J., 2006. Application of multi-temporal differential interferometry to slope instability detection in urban/peri-urban areas, *Eng. Geol.*, **88**, 218–239.
- Bürgmann, R., Hilley, G., Ferretti, A. & Novali, F., 2006. Resolving vertical tectonics in the San Francisco Bay area from permanent scatterer InSAR and GPS analysis, *Geology*, **34**, 221–224.
- Burrato, P., Ciucci, F. & Valensise, G., 2003. An inventory of river anomalies in the Po Plain, Northern Italy: evidence for active blind thrust faulting, *Ann. Geophys.*, **5**, 865–882.
- Burrato, P., Vannoli, P., Fracassi, U., Basili, R. & Valensise, G., 2012. Is blind faulting truly invisible? Tectonic-controlled drainage evolution in the epicentral area of the May 2012, Emilia-Romagna earthquake sequence (Northern Italy), *Ann. Geophys.*, **55**(4), 525–531.
- Calda, N., Valloni, R. & Bedulli, F., 2007. Three-dimensional representation of permeability barriers and aquifers recharge in the pleistocene deposits of the Parma Alluvial Plain, *Mem. Descr. Carta Geol. d'It.*, **LXXVI**, 97–108.
- Carminati, E. & Martinelli, G., 2002. Subsidence rates in the Po Plain, northern Italy: the relative impact of natural and anthropogenic causation, *Eng. Geol.*, **66**, 241–255.

- Caro Cuenca, M., Hanssen, R.F., Hooper, A. & Arikan, M., 2012. Surface deformation of the whole Netherlands after PSI analysis, in *Proceedings of Fringe 2011 Workshop*, Vol. SP-697, ed. Ouweland, L., 19–23 September 2011, ESA Publications, Frascati, Italy.
- Castiglioni, G.B., Bondesan, A., Bondesan, M., Cavallin, A., Gasperi, G. & Persico, A., 1997. *Geomorphological Map of the Po Plain, Map of Relief and Vertical Movements of Po Plain (1 : 250.000 scale)*, S.EL.CA., Firenze.
- Cenni, N., Mantovani, E., Baldi, P. & Viti, M., 2012. Present kinematics of Central and Northern Italy from continuous GPS measurements, *J. Geodyn.*, **58**, 62–72.
- Cenni, N., Viti, M., Baldi, P., Mantovani, E., Bacchetti, M. & Vannucchi, A., 2013. Present vertical movements in Central and Northern Italy from GPS data: possible role of natural and anthropogenic causes, *J. Geodyn.*, **7**, 74–85.
- Cenni, N. *et al.*, 2014. The spatio-temporal pattern of subsidence in the Po basin monitored by different techniques, in *Proceedings of 33<sup>rd</sup> Convegno Nazionale GNGTS*, 001–260, Vol. 1, pp. 134–139.
- Champenois, J., Fruneau, B., Pathier, E., Deffontaines, B., Lin, K.-C. & Hu, J.-C., 2012. Monitoring of active tectonic deformations in the Longitudinal Valley (eastern Taiwan) using Persistent Scatterer InSAR method with ALOS PALSAR data, *Earth planet. Sci. Lett.*, **337**, 144–155.
- Chen, C.-T., Hu, J.-C., Lu, C.-Y., Lee, J.-C. & Chan, Y.-C., 2007. Thirty-year land elevation change from subsidence to uplift following the termination of groundwater pumping and its geological implications in the Metropolitan Taipei Basin, Northern Taiwan, *Eng. Geol.*, **95**, 30–47.
- Ciaccio, M.G. & Chiarabba, C., 2002. Tomographic models and seismotectonics of the Reggio Emilia region, Italy, *Tectonophysics*, **344**, 261–276.
- Colesanti, C. & Wasowski, J., 2006. Investigating landslides with satellite Synthetic Aperture Radar (SAR) interferometry, *Eng. Geol.*, **88**(3–4), 173–199.
- Costantini, M., Iodice, A., Magnapane, L. & Pietranera, L., 2000. Monitoring terrain movements by means of sparse SAR differential interferometric measurements, in *Proceedings of 20th IEEE International Geoscience and Remote Sensing Symposium (IGARSS'00)*, 24–28 July 2000, pp. 3225–3227, Honolulu, Hawaii, USA.
- Cremonini, G. & Ricci Lucchi, F., 1982. Guida alla geologia del margine appenninico-padano, in *Guide Geologiche Regionali*, Società Geologica Italiana, 248 pp.
- Crosetto, M., Monserrat, O., Bremmer, C., Hanssen, R., Capes, R. & Marsh, S., 2008. Ground motion monitoring using SAR interferometry: quality assessment, *Eur. Geol.*, **26**, 12–15.
- Crosetto, M., Monserrat, O., Cuevas, M. & Crippa, B., 2011. Spaceborne differential SAR interferometry: data analysis tools for deformation measurement, *Remote Sens.*, **3**(2), 305–318.
- Crosetto, M., Monserrat, O., Cuevas-González, M., Devanthéry, N. & Crippa, B., 2016. Persistent scatterer interferometry: a review, *ISPRS J. Photogram. Remote Sens.*, **11**, 78–89.
- Cuffaro, M., Riguzzi, F., Scrocca, D., Antonioli, F., Carminati, E., Divani, M. & Doglioni, C., 2010. On the geodynamics of the Northern Adriatic Plate, *Rend. Fis. Acc. Lincei*, **21**(1), S253–S279.
- D'Agostino, N., Avallone, A., Cheloni, D., D'anastasio, E., Mantenuto, S. & Selvaggi, G., 2008. Active tectonics of the Adriatic region from GPS and earthquake slip vectors, *J. geophys. Res.*, **113**, B12413, doi:10.1029/2008JB005860.
- Davis, J.L., Wernicke, B.P. & Tamisiea, M.E., 2012. On seasonal signals in geodetic time series, *J. geophys. Res.*, **117**(B1), 1–10.
- Del Ventisette, C., Righini, G., Moretti, S. & Casagli, N., 2014. Multitemporal landslides inventory map updating using spaceborne SAR analysis, *Int. J. Appl. Earth Observ. Geoinform.*, **30**(1), 238–246.
- Devanthéry, N., 2014. High-resolution deformation measurement using “Persistent Scatterer Interferometry”, *PhD thesis*, Technical University of Catalonia, 77 pp.
- Devanthéry, N., Crosetto, M., Monserrat, O., Cuevas-González, M. & Crippa, B., 2014. An approach to Persistent Scatterer Interferometry: the PSIG chain, *Remote Sens.*, **6**, 6662–6679.
- Devoti, R., Esposito, A., Pietranterio, G., Pisani, A.R. & Riguzzi, F., 2011. Evidence of large scale deformation patterns from GPS data in the Italian subduction boundary, *Earth planet. Sci. Lett.*, **311**(3–4), 230–241.
- DISS Working Group, 2010. *Database of Individual Seismogenic Sources (DISS), Version 3.1.1: A Compilation of Potential Sources for Earthquakes Larger Than M 5.5 in Italy and Surrounding Areas*, INGV (Istituto Nazionale di Geofisica e Vulcanologia).
- Fattahi, H. & Amelung, F., 2014. InSAR uncertainty due to orbital errors, *Geophys. J. Int.*, **199**(1), 549–560.
- Ferretti, A., Prati, C. & Rocca, F., 2001. Permanent scatterers in SAR interferometry, *IEEE Trans. Geosci. Remote Sens.*, **39**(1), 8–20.
- Ferretti, A., Savio, G., Barzaghi, R., Borghi, A., Musazzi, S., Novali, F., Prati, C. & Rocca, F., 2007. Submillimeter accuracy of InSAR time series: experimental validation, *IEEE Trans. Geosci. Remote Sens.*, **45**(5), 1142–1153.
- Ferretti, A., Fumagalli, A., Novali, F., Prati, C., Rocca, F. & Rucci, A., 2011. A new algorithm for processing interferometric data-stacks: SqueeSAR, *IEEE Trans. Geosci. Remote Sens.*, **49**(9), 3460–3470.
- Fuhrmann, T., Caro Cuenca, M., Knöpfler, A., van Leijen, F. J., Mayer, M., Westerhaus, M., Hanssen, R. F. & Heck, B., 2015. Estimation of small surface displacements in the Upper Rhine Graben area from a combined analysis of PS-InSAR, levelling and GNSS data, *Geophys. J. Int.*, **203**(1), 614–631.
- Gambolati, G. & Teatini, P., 2015. Geomechanics of subsurface water withdrawal and injection, *Water Resour. Res.*, **51**, 3922–3955.
- Gatto, P. & Carbognin, L., 1981. The Lagoon of Venice: natural environmental trend and man-induced modification, *Hydrol. Sci.-Bul.*, **26**(4), 379–391.
- Ghielmi, M., Minervini, M., Nini, C., Rogledi, S. & Rossi, M., 2013. Late Miocene–Middle Pleistocene sequences in the Po Plain—Northern Adriatic Sea (Italy): the stratigraphic record of modification phases affecting a complex foreland basin, *Mar. Pet. Geol.*, **42**, 50–81.
- Grandin, R., Doin, M.P., Bollinger, L., Pinel-Puysségur, B., Ducret, G., Jolivet, R. & Sapkota, S.N., 2012. Long-term growth of the Himalaya inferred from interseismic InSAR measurement, *Geology*, **40**(12), 1059–1062.
- Guidoboni, E., Ferrari, G., Mariotti, D., Comastri, A., Tarabusi, G. & Valensise, G., 2007. CFTI4Med, catalogue of strong earthquakes in Italy (461 B.C.–1997) and Mediterranean Area (760 B.C.–1500). Available at: <http://storing.ingv.it/cfti4med/>, last accessed 6 April 2016.
- Gunderson, K.L. *et al.*, 2014. Unraveling tectonic and climatic controls on synorogenic growth strata (Northern Apennines, Italy), *GSA Bull.*, **126**(3/4), 532–552.
- Hanssen, R.F., 2001. Radar interferometry: data interpretation and error analysis, *PhD thesis*, Tech. Univ., Delft; Kluwer Academic, Dordrecht, The Netherlands.
- Hanssen, R.F., van Leijen, F.J., van Zwielen, G.J., Bremmer, C., Dortal, S. & Kleuskens, M., 2008. Validation of existing processing chains in TerraFirma stage 2; Product validation: validation in the Amsterdam and Alkmaar area, in *GMES TerraFirma Report*, ESRIN/contract No. 19366/05/I-E, Delft University of Technology, The Netherlands, 85 pp.
- Hilley, G.E., Bürgmann, R., Ferretti, A., Novali, F. & Rocca, F., 2004. Dynamics of slow-moving landslides from Permanent Scatterer analysis, *Science*, **304**(5679), 1952–1955.
- Hooper, A., Zebker, H.A., Segall, P. & Kampes, B.M., 2004. A new method for measuring deformation on volcanoes and other natural terrains using InSAR persistent scatterers, *Geophys. Res. Lett.*, **31**, L23611, doi:10.1029/2004GL021737.
- ISIDE Working Group, 2010. Italian seismological instrumental and parametric database. Available at: <http://iside.rm.ingv.it>, last accessed 4 April 2016.
- Kampes, B.M., 2006. *Radar Interferometry: Persistent Scatterer Technique*, Springer.
- Lagios, E., Sakkas, V., Novali, F., Bellotti, F., Ferretti, A., Vlachou, K. & Dietrich, V., 2013. SqueeSAR<sup>TM</sup> and GPS ground deformation monitoring of Santorini Volcano (1992–2012): tectonic implications, *Tectonophysics*, **594**, 38–59.



- Janari, R., Mora, O., Manunta, M., Mallorqui, J.J., Berardino, P. & Sansosti, E., 2004. A small baseline approach for investigating deformation on full resolution differential SAR interferograms, *IEEE Trans. Geosci. Remote Sens.*, **42**, 1377–1386.
- Lyons, S. & Sandwell, D., 2003. Fault creep along the southern San Andreas from interferometric synthetic aperture radar, permanent scatterers, and stacking, *J. geophys. Res.*, **108**(B1), 2047, doi:10.1029/2002JB001831.
- Maesano, F., D'ambrogio, C., Burrato, P. & Toscani, G., 2015. Slip-rates of blind thrusts in the Po sedimentary basin (Northern Apennines, Italy), *Tectonophysics*, **643**, 8–25.
- Mariotti, G. & Doglioni, C., 2000. The dip of the foreland monocline in the Alps and Apennines, *Earth planet. Sci. Lett.*, **181**, 191–202.
- Martín, P.E., Herrera, G., Sacristán, M.M., Tomás, R., Béjar-Pizarro, M. & Marin, R.M., 2014. A quasi-elastic aquifer deformational behavior: Madrid aquifer case study, *J. Hydrol.*, **519**, 1192–1204.
- Massironi, M., Zampieri, D., Bianchi, M., Schiavo, A. & Franceschini, A., 2009. Use of PSInSAR<sup>TM</sup> data to infer active tectonics: clues on the differential uplift across the Giudicarie belt (Central-Eastern Alps, Italy), *Tectonophysics*, **476**, 297–303.
- Massonnet, D. & Feigl, K.L., 1998. Radar interferometry and its applications to changes in the Earth's surface, *Rev. Geophys.*, **36**, 441–500.
- Massonnet, D., Rossi, M., Carmona, C., Adragna, F., Peltzer, G., Feigl, K. & Rabaute, T., 1993. The displacement field of the Landers earthquake mapped by radar interferometry, *Nature*, **364**, 138–142.
- Meisina, C., Zucca, F., Notti, D., Colombo, A., Cucchi, G., Giannico, C. & Bianchi, M., 2008. Geological interpretation of PSInSAR data at regional scale, *Sensors*, **8**(11), 7469–7492.
- Michetti, A.M. *et al.*, 2012. Active compressional tectonics, Quaternary capable faults, and the seismic landscape of the Po Plain (northern Italy), *Ann. Geophys.*, **55**(5), 969–1001.
- Monserrat, O., 2012. Deformation measurement and monitoring with ground-based SAR, *PhD thesis*, Technical University of Catalonia.
- Montone, P., Mariucci, M.T. & Pierdominici, S., 2012. The Italian present-day stress map, *Geophys. J. Int.*, **189**(2), 705–716.
- Mora, O., Mallorqui, J.J. & Broquetas, A., 2003. Linear and nonlinear terrain deformation maps from a reduced set of interferometric SAR images, *IEEE Trans. Geosci. Remote Sens.*, **41**, 2243–2253.
- Pagli, C., Sigmundsson, F., Arnadóttira, T., Einarsson, P. & Sturkell, E., 2006. Deflation of the Askja volcanic system: constraints on the deformation source from combined inversion of satellite radar interferograms and GPS measurements, *J. Volcanol. Geotherm. Res.*, **152**, 97–108.
- Pedersen, R., Jónsson, S., Arnadóttir, T., Sigmundsson, F. & Feigl, K.L., 2003. Fault slip distribution of two June 2000 MW6.5 earthquakes in South Iceland estimated from joint inversion of InSAR and GPS measurements, *Earth planet. Sci. Lett.*, **213**, 487–502.
- Perrone, G. *et al.*, 2013. Current tectonic activity and differential uplift along the Cottian Alps/Po Plain boundary (NW Italy) as derived by PS-InSAR data, *J. Geodyn.*, **66**, 65–78.
- Petrucci, F., Bigi, B., Cavazzini, R., Moretori, L., Panici, E., Pecorari, M. & Rossetti, G., 1975. Ricerche sulle acque sotterranee della pianura parmense e piacentina: sezioni interpretative degli acquiferi (parte prima), in *Pubblicazioni Istituto di Geologia Università di Parma*, p. 14, Grafiche STEP Editrice Parma.
- Peyret, M., Masson, F., Yavasoglu, H., Ergintav, S. & Reilinger, R., 2013. Present-day strain distribution across a segment of the central bend of the North Anatolian Fault Zone from a Persistent-Scatterers InSAR analysis of the ERS and Envisat archives, *Geophys. J. Int.*, **192**, 929–945.
- Pezzo, G. *et al.*, 2013. Coseismic deformation and source modeling of the May 2012 Emilia (Northern Italy) earthquakes, *Seismol. Res. Lett.*, **84**(4), 645–655.
- Pezzo, G., Tolomei, C., Atzori, S., Salvi, S. & Merryman Boncori, J.P., 2014. Seismic cycle measurements from SAR interferometry: inter-, co- and post-seismic deformation associated to the 2012 Emilia seismic sequence, in *Proceedings of the 33<sup>rd</sup> Convegno Nazionale GNGTS*, 001–260, Vol. 1, pp. 107–113.
- Pieri, M. & Groppi, G., 1981. Subsurface geological structure of the Po Plain, Italy, in *Un Progetto Finalizzato Geodinamica*, p. 414, C.N.R. Publications.
- Pondrelli, S., Salimbeni, S., Ekstrom, G., Morelli, A., Gasperini, P. & Vannucci, G., 2006. The Italian CMT dataset from 1977 to the present, *Phys. Earth Planet.*, **159**(3–4), 286–303.
- Pondrelli, S., Salimbeni, S., Perfetti, P. & Danecek, P., 2012. Quick regional centroid moment tensor solutions for the Emilia 2012 (northern Italy) seismic sequence, *Ann. Geophys.*, **55**, 615–621.
- Price, E. & Sandwell, D.T., 1998. Small-scale deformations associated with the 1992 Landers, California Earthquake mapped by synthetic aperture radar interferometry phase gradients, *J. geophys. Res.*, **103**, 27 001–27 016.
- Regione Emilia-Romagna, and ENI AGIP, 1998. *Riserve Idriche Sotterranee Della Regione Emilia-Romagna*, Società Elaborazioni Cartografiche, 119 pp.
- Ricci Lucchi, F., Colalongo, M.L., Cremonini, G., Gasperi, G., Iaccarino, S., Papani, G., Raffi, I. & Rio, D., 1982. Evoluzione sedimentaria e paleogeografica del margine appenninico, in *Guide Geologiche Regionali*, pp. 17–46, Società Geologica Italiana.
- Righini, G., Pancioli, V. & Casagli, N., 2012. Updating landslide inventory maps using Persistent Scatterers Interferometry (PSI), *Int. J. Remote Sens.*, **33**(7), 2068–2096.
- Righini, G., Raspini, F., Moretti, S. & Cigna, F., 2011. Unsustainable use of groundwater resources in agricultural and urban areas: a persistent scatterer study of land subsidence at the basin scale, in *WIT Transactions on Ecology and the Environment*, Vol. 144, pp. 81–92, WIT Press.
- Rovida, A., Camassi, R., Gasperini, P. & Stucchi, M., 2011. *CPT111, the 2011 Version of the Parametric Catalogue of Italian Earthquakes*, Milano, Bologna, doi:10.6092/INGV.IT-CPT11.
- Samiee-Esfahany, S., Hanssen, R. F., van Thienen-Visser, K. & Muntendam-Bos, A., 2010. On the effect of horizontal deformation on InSAR subsidence estimates, in *Proceedings of Fringe 2009 Workshop*, ed. Lacoste, H., Vol. SP-677, 30 November–4 December 2009, ESA Publications, Frascati, Italy.
- Schmidt, D. A. & Bürgmann, R., 2003. Time dependent land uplift and subsidence in the Santa Clara Valley, California, from a large InSAR data set, *J. geophys. Res.*, **108**(B9), 2416, doi:10.1029/2002JB002267.
- Scognamiglio, L. *et al.*, 2012. The 2012 Pianura Padana Emiliana seismic sequence: locations, moment tensors and magnitudes, *Ann. Geophys.*, **55**(4), doi:10.4401/ag-6159.
- Scrocca, D., Carminati, E., Doglioni, C. & Marcantoni, D., 2007. Slab retreat and active shortening along the Central-Northern Apennines, in *Thrust Belts and Foreland Basins: Frontiers in Earth Sciences*, Springer, pp. 471–487.
- Stramondo, S. *et al.*, 2007. Surface movements in Bologna (Po Plain, Italy) detected by multitemporal DInSAR, *Remote Sens. Environ.*, **110**, 304–316.
- Strozzi, T., Tosi, L., Wegmüller, U., Teatini, P. & Carbognin, L., 2001. Thematic and land subsidence maps of the Lagoon of Venice from ERS SAR interferometry, in *CoRiLa Research Program 2001 Results*, pp. 345–355, ed. Campostrini, P., IVSLA Venezia.
- Strozzi, T. *et al.*, 2005. Survey and monitoring of landslide displacements by means of L-band satellite SAR interferometry, *Landslides*, **2**(3), 193–201.
- Tizzani, R. *et al.*, 2013. New Insights Into The 2012 Emilia (Italy) Seismic sequence through advanced numerical modeling of ground deformation InSAR measurements, *Geophys. Res. Lett.*, **40**(10), 1971–1977.
- Tolomei, C., Salvi, S., Merryman Boncori, J.P. & Pezzo, G., 2015. InSAR measurement of crustal deformation transients during the earthquake preparation processes: a review, *Boll. Geof. Teor. Appl.*, **56**(2), 151–166.
- Toscani, G., Burrato, P., Di Bucci, D., Seno, S. & Valensise, G., 2009. Plio-Quaternary tectonic evolution of the northern Apennines thrust fronts (Bologna-Ferrara section, Italy): seismotectonic implications, *Ital. J. Geosci.*, **128**, 605–613.
- Valensise, G. & Pantosti, D., 2001. Database of potential sources for earthquakes larger than M 5.5 in Italy, *Ann. Geof.*, **44**(4), 180, doi:10.4401/ag-3562.
- Vannoli, P., Burrato, P. & Valensise, G., 2015. The seismotectonics of the Po Plain (northern Italy): tectonic diversity in a blind faulting domain, *Pure appl. Geophys.*, **172**, 1105–1142.

- ViDEPI database. Available at: <http://unmig.sviluppoeconomico.gov.it/videpi/cessati/sismica.titoli.asp>.
- Vilardo, G., Ventura, G., Terranova, C., Matano, F. & Nardò, S., 2009. Ground deformation due to tectonic, hydrothermal, gravity, hydrogeological, and anthropic processes in the Campania Region (Southern Italy) from Permanent Scatterers Synthetic Aperture Radar Interferometry, *Remote Sens. Environ.*, **113**, 197–212.
- Waltham, T., 2002. Sinking cities—feature, *Geol. Today*, **18**(3), 95–100.
- Werner, C., Wegmüller, U., Strozzi, T. & Wiesmann, A., 2003. Interferometric point target analysis for deformation mapping, in *Proceedings of IGARSS 2003*, Vol. 7, pp. 4362–4364.
- Wright, T.J., Parsons, B., England, P.C. & Fielding, E.J., 2004. InSAR observations of low slip rates on the major faults of Western Tibet, *Science*, **305**(5681), 236–239.
- Wright, T.J. *et al.*, 2012. Geophysical constraints on the dynamics of spreading centers from rifting episodes on land, *Nat. Geosci.*, **5**(4), 242–250.
- Zebker, H.A. & Villasenor, J., 1992. Decorrelation in interferometric radar echoes, *IEEE Trans. Geosci. Remote Sens.*, **30**, 950–959.
- Zerbini, S., Richter, B., Rocca, F., van Dam, T. & Matonti, F., 2007. A combination of space and terrestrial geodetic techniques to monitor land subsidence: case study, the Southeastern Po Plain, Italy, *J. geophys. Res.*, **112**, B05401, doi:10.1029/2006jb004338.